

Particulate trace element distributions along the Canadian Arctic GEOTRACES section: shelf-water interactions, advective transport and contrasting biological production

Manuel Colombo^{1,*}, Jingxuan Li¹, Birgit Rogalla, Susan E. Allen,
Maria T. Maldonado

Department of Earth, Ocean, and Atmospheric Sciences, University of British Columbia, BC V6T 2Z4, Canada

Received 26 June 2021; accepted in revised form 11 February 2022; Available online 17 February 2022

Abstract

Marine particles are important regulators of the biogeochemistry of many trace elements and isotopes in the ocean, and as such, there has been an increasing motivation to unravel the processes which control their cycling. Here, we present vertical distributions of total particulate trace elements (Al, V, Fe, Mn and P) and particulate organic carbon and particulate nitrogen (POC and pN) collected during the GEOTRACES Canadian cruise in 2015 in the Canada Basin (CB), the Canadian Arctic Archipelago (CAA), Baffin Bay (BB) and the Labrador Sea (LS), where particulate trace metal data are scarce. While particulate trace elements are generally affected by one-dimensional dynamics in ocean waters (e.g. deposition, scavenging/remineralization, and sinking), lateral transport of lithogenic-derived particles (pAl, pV and pFe) plays a dominant role in shaping their distributions in the deep CB, BB and LS basins. Higher concentrations of the aforementioned particulate trace elements are measured along the flow path of boundary currents and in near-bottom waters. Unlike pAl, pV and pFe, primarily controlled by lithogenic sources, bulk pMn distributions in our study regions (with the exception of LS) are dominated by authigenic $\text{Mn}^{+3/4}$ oxides, with distinctively high concentrations in CB and BB subsurface halocline waters, as well as in the deepest samples in BB. Enhanced bacterially-mediated Mn^{+2} oxide formation is anticipated to occur in these halocline waters which have the potential to sustain large populations of Mn oxidizing bacteria as result of the close sediment-water interactions and distinct environmental conditions of these water masses. Overall, the highest concentrations of pP, POC and pN occurred in surface and near-surface waters (>100 m) at the same density as a chlorophyll-a peak and transmissivity drop, with a clear west-east increasing concentration gradient from the CB to LS. In summary, biogeochemical cycles of particulate elements in the Canadian Arctic Ocean are controlled by enhanced lateral transport and sediment resuspension (pAl, pFe and pV), authigenic formation of Mn and biological production (pP, POC and pN).

© 2022 Elsevier Ltd. All rights reserved.

Keywords: Advective transport; Lithogenic sources; Particle dynamics; Sediment resuspension; Trace metal biogeochemistry; Canadian Arctic Ocean; Redfield stoichiometry; GEOTRACES

1. INTRODUCTION

Marine particles – operationally defined as material collected onto 0.2–0.4 μm pore size filters – are important trace metal reservoirs, largely exceeding the dissolved pool in shelf regions, which strongly modulate oceanic

* Corresponding author.

E-mail address: manuel.colombo@alumni.ubc.ca (M. Colombo).

¹ Current Address: Department of Marine Chemistry and Geochemistry, Woods Hole Oceanographic Institution, 360 Woods Hole Road, Woods Hole, MA 02543-1543, USA

biogeochemistry by controlling the residence time of most elements (Lam and Bishop, 2008; Jeandel et al., 2015; Ohnemus and Lam, 2015; Homoky et al., 2016; Jeandel, 2016). Particulate material is a heterogeneous phase, with diverse sources and complex composition. Lithogenic particles, derived from weathering and erosion of the continental crust, are primarily delivered to ocean waters by means of atmospheric deposition (Mahowald et al., 2018), river discharge (Aguilar-Islas et al., 2013; Jeandel and Oelkers, 2015; Charette et al., 2016; Jeandel, 2016; Colombo et al., 2019a) and sea ice melt (Measures, 1999; Tovar-Sánchez et al., 2010; Aguilar-Islas et al., 2013; Giesbrecht et al., 2013). Mid-depth lateral transport of continental margin sediments and near-bottom sediment resuspension events are also important sources of lithogenic particulate trace elements (e.g. Al, Ti, V, Fe) to the water column (Lam and Bishop, 2008; Jeandel et al., 2015; Ohnemus and Lam, 2015; Charette et al., 2016; Jeandel, 2016; Gourain et al., 2019; Morton et al., 2019). In addition to lithogenic sources, vast quantities of biogenic marine particles are produced in surface waters through the assimilation of dissolved carbon, macronutrients (e.g. silicic acid, nitrate, phosphate) and micronutrients (e.g. Mn, Fe, Co, Ni, Cu, Zn, Cd) by phytoplankton (Jeandel et al., 2015; Lam et al., 2015; Twining et al., 2015; Yigiterhan et al., 2011). Moreover, authigenic particles such as Fe and Mn oxides, are generated at the ocean floor above reducing sediment conditions and in the water column where dissolved species of redox-sensitive elements are oxidized, producing particles enriched in these elements over their crustal abundances (Lam and Bishop, 2008; Yigiterhan et al., 2011; Hansel, 2017; Oldham et al., 2017; Morton et al., 2019; Vieira et al., 2019).

Given the relevance of particles in the cycling of trace elements and isotopes (TEIs), the fact that many particulate TEIs are useful tracers of biogeochemical and physical ocean processes, and, as TEIs dissolve and/or remineralize, they release important micronutrients for phytoplankton (Lam and Bishop, 2008; Jeandel et al., 2011; Anderson et al., 2014; Jeandel and Oelkers, 2015; Cheize et al., 2019), the study of particulate trace element distributions is one of the main objectives of the international GEOTRACES program. In recent years, large oceanographic campaigns, framed within the international GEOTRACES program, have shed light on the biogeochemistry of particulate trace elements on the North Atlantic Zonal Transect (Lam et al., 2015; Ohnemus and Lam, 2015; GA03 GEOTRACES cruise), the Eastern Pacific Zonal Transect (Ohnemus et al., 2017; Lam et al., 2018; Lee et al., 2018; GP16 GEOTRACES cruise), and the North Subarctic Atlantic from the Iberian margin to the Labrador Sea (Gourain et al., 2019; GEOTRACES GA01 cruise). Nonetheless, our knowledge of particulate trace metal distributions in other regions, such as the Arctic Ocean, is still very limited. A handful of studies have reported concentrations of total dissolvable trace metals in the Chukchi Sea and adjacent shelf break areas of the Canada Basin, however, these studies focused on the leachable fraction of the particulate pool (Thuróczy et al., 2011; Cid et al., 2012; Giesbrecht et al., 2013; Kondo et al., 2016; Vieira et al.,

2019). To the best of our knowledge, three studies have described the distributions of particulate elements in the Chukchi Sea and Western Arctic Ocean (GN01 GEOTRACES cruise; Aguilar-Islas et al., 2013; Whitmore et al., 2019; Xiang and Lam, 2020), and three other studies have reported particulate organic carbon distributions in the Canada Basin (Trimble and Baskaran, 2005; Jackson et al., 2010; Brown et al., 2014).

This study contributes to the growing body of literature by presenting spatial and vertical distributions of total particulate trace elements (pAl, pV, pFe, pMn and pP) and particulate organic carbon and particulate nitrogen (POC and pN) across the deep Canada Basin, Baffin Bay and Labrador Sea, as well as pP, POC and pN distributions in the shallow Canadian Arctic Archipelago. With the aid of ancillary data, modeled tidal stresses and particle tracking simulations, we unravel the sources and processes shaping particulate distributions in the unique Canadian Arctic Ocean, a land-influenced environment characterized by extensive continental margins and shelves.

2. STUDY AREA AND HYDROGRAPHY

The Canada Basin is strongly salinity stratified, with a fresh polar mixed layer (PML), seasonally modified by freeze-thaw cycles of sea ice and snow, and a multilayered halocline (~30–400 m) which insulates the PML from the underlying saltier and warmer Atlantic Layer (AL). The halocline assembly consists of the Alaskan Coastal Water (ACW), with a potential temperature (θ) of about $\sim 0^\circ\text{C}$ and a salinity (S) range of $30 < S < 32$, a relatively saltier ($32 < S < 33$) summer Bering Sea Water (sBSW) occupying the bulk of the central Chukchi Sea, and the winter Bering Sea Water (wBSW), distinguished by a weak temperature minimum near $S = 33.1$, which is advected from Bering Strait and contributes to the middle halocline layer (Steele et al., 2004; McLaughlin et al., 2005; Timmermans et al., 2017; Fig. 1 and Figure S1a in the supporting information). Unlike the upper and middle halocline, the lower halocline (LH) consists mostly of Atlantic-origin waters, and is identified by a sharp increase in temperature at salinities between 33.3 and 34.6 (McLaughlin et al., 2005; Shimada et al., 2005; Woodgate and Aagaard, 2005). The AL (~400–1200 m) has two components: the Fram Strait Branch (FSB), distinguished by a temperature maximum and the Barents Sea Branch (BSB), which is deeper and colder (Smethie et al., 2000; McLaughlin et al., 2004; Aksenov et al., 2011). Underlying the AL lies the old, cold and more saline Canada Basin Deep Water (CBDW > 1200 m; Timmermans et al., 2003; Figs. 1 and S1a).

The Canadian Arctic Archipelago (CAA) is a complex network of islands and shallow straits, connecting the Arctic Ocean to Baffin Bay. This shelf dominated region is an important export conduit for fresh and nutrient rich Pacific waters (phosphate, silicic acid and bio-active trace metals) to the North Atlantic, enhancing the productivity downstream (Michel et al., 2006; Beszczynska-Möller et al., 2011; Wang et al., 2012; Hill et al., 2013; Colombo et al., 2021). The CAA links the Arctic Ocean with Baffin Bay

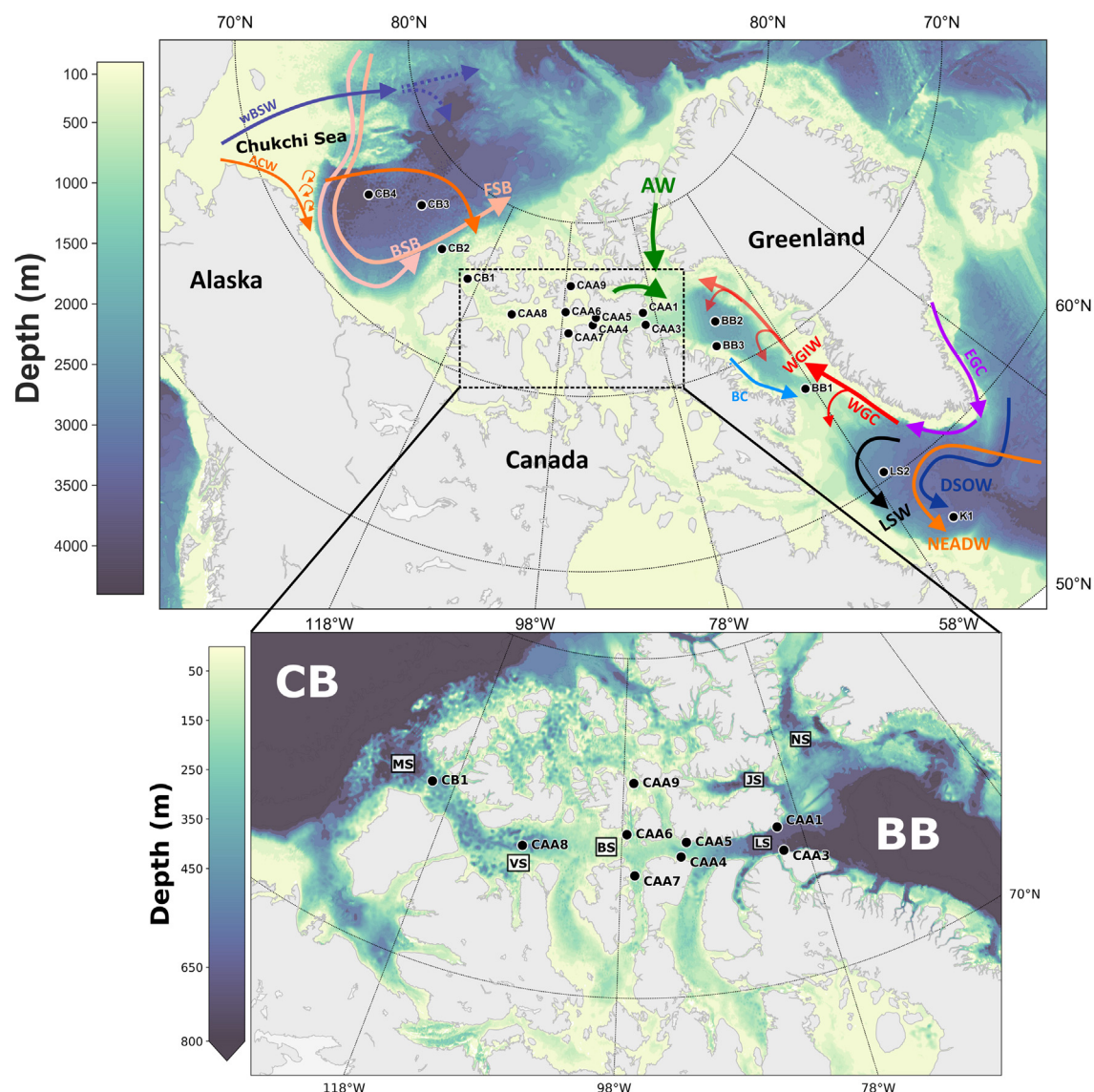


Fig. 1. Sampled stations for particulate trace elements, organic carbon and nitrogen during the Canadian Arctic GEOTRACES cruises (GN02 and GN03), alongside bathymetry and a schematic of water circulation in the Canada Basin (after [Aksenov et al., 2011](#); [Kondo et al., 2016](#)) and Baffin Bay and the Labrador Sea (after [Yashayaev and Clarke, 2008](#); [Curry et al., 2011](#); [Lozier et al., 2017](#)). ACW: Alaskan Coastal Water, wBSW: winter Bering Sea Water, FSB: Fram Strait Branch, BSB: Barents Sea Branch, AW: Arctic Water, EGC: East Greenland Current, WGC: West Greenland Current, WGIW: West Greenland Intermediate Water, BC: Baffin Current, LSW: Labrador Sea Water, NSDW: Northeast Atlantic Deep Water, DSOW: Denmark Strait Overflow Water. Canada Basin stations: CB2–CB4, Canadian Arctic Archipelago stations: CB1 and CAA1–CAA9 (only particulate phosphorus, organic carbon and nitrogen data from the CAA are presented in this study), Baffin Bay stations: BB1–BB3, Labrador Sea stations: LS2 and K1. Landmarks and straits of the Canadian Arctic Archipelago are displayed in the inset; MS: M'Clure Strait, VS: Viscount Melville Sound, BS: Barrow Strait, LS: Lancaster Sound, NS: Nares Strait, JS: Jones Sound. Parry Channel is the main pathway in central CAA connecting M'Clure Strait with Lancaster Sound.

by three main pathways: 1- Parry Channel (sill depth: ~120 m), running from M'Clure Strait to Lancaster Sound, where Arctic Water (AW) is exported to Baffin Bay, 2- Nares Strait (sill depth: ~220 m), and 3- Jones Sound (sill depth: ~125 m; [Fig. 1](#)).

Baffin Bay is connected to the Labrador Sea and the North Atlantic Ocean through Davis Strait (~650 m). The overall circulation in this bay is cyclonic, with a northward flow on the eastern side of Davis Strait, the West Greenland Current (WGC), which consists of subsurface

freshwater of Arctic origin (East Greenland Current), and the warm and salty West Greenland Intermediate Water (WGIW: ~300–800 m; $\theta > 1.3$ °C and $S > 34.2$) of North Atlantic origin ([Cuny et al., 2005, 2011](#); [Lozier et al., 2017](#)). This northward inflow is modified during its cyclonic circulation, and the upper layers of the WGC are mixed with Arctic Waters, resulting in the fresh and cold Arctic Water (AW; $\theta < 0$ °C and $32.0 < S < 33.7$), which continues its flow to the Labrador Sea as the Baffin Current ([Tang et al., 2004](#); [Cuny et al., 2005](#)). Underlying the WGIW, lies

the Baffin Bay Deep Water (BBDW), which is characterized by a small change in salinity and a steady decrease in potential temperature (Tang et al., 2004; Figs. 1 and S1c).

The subsurface circulation in the Labrador Sea is cyclonic, consisting of two components: the WGC and the Labrador Current. The Labrador Current flows southward along the Labrador Shelf and Slope and is the extension of the Baffin Current (BC; Cuny et al., 2002; Fischer et al., 2004). The Labrador Sea Water (LSW) lies between the subsurface water and the deep western boundary current. Two LSW classes were distinguished from the CTD data in 2015: the newly ventilated and fresher LSW formed during the winters of 2014 and 2015 (LSW-2015), and the oldest, saltiest and least oxygenated LSW produced in the winters of 1987–1994 (LSW-87/94; Yashayaev and Loder, 2016). Underlying the LSW-87/94, lies the saline, warm ($\theta \sim 3^\circ\text{C}$, $S \sim 34.92$) and less oxygenated Northeast Atlantic Deep Water (NSDW), and the deepest, less saline, colder ($\theta \leq 2.6^\circ\text{C}$, $S \sim 34.9$) and more-recently oxygenated Denmark Strait Overflow Water (DSOW; Yashayaev et al., 2007; Yashayaev and Loder, 2016; Figs. 1 and S1d).

3. METHODS

3.1. Sample collection

Samples were collected on the *CCGS Amundsen* as part of GEOTRACES sections GN02 and GN03 (10/07/2015–1/10/2015) which covered an area from 56°N to 77°N and 53°W to 150°W in the Canadian Arctic. The sampling was carried out during summer and early fall months, and hence, most stations were ice-free when seawater samples were collected (Colombo et al., 2020). Vertical profiles ranging from approximately 10 to 3500 m depth were obtained at 17 stations: three in the Canada Basin, nine in the CAA (only pP, POC and pN distributions from the CAA are discussed in this paper), three in Baffin Bay and two in the Labrador Sea (Fig. 1). A trace-metal clean sampling system consisting of a powder-coated aluminum frame, which held twelve 12 L Teflon-coated GO-FLO bottles (General Oceanics, Miami FL USA) and a SeaBird 911 CTD/SBE 43 oxygen sensor instrument package (Seabird Electronics Inc, Bellevue WA USA), attached by a 4000 m 4-member conducting Vectran cable encased in polyurethane (Cortland Cable Co., Cortland NY USA) was used to collect seawater samples for particulate trace element analysis.

On-board the ship, these samples were transferred to a trace metal clean sampling van (HEPA filtered environment), where ten liters of unfiltered seawater were collected into pre-cleaned 10 L LDPE cubitainers (Bel Art and Nalgene) by the use of a piece of C-flex tubing (Masterflex) together with a Teflon straw. Seawater was then filtered through a $0.45\ \mu\text{m}$ Supor filter (47 mm diameter) inside a HEPA-filtered clean air bubble. The filtration system included a cubitainer, a spigot, C-flex tubing, a peristaltic pump (Cole-Palmer), a 47 mm filter holder (Millipore) with customized screws, waste tubing and a waste container for volume recording. After filtration, filters were dried inside a laminar flow hood, folded in half, and stored in clean poly

bags until analysis. Supor filters were always handled using pre-cleaned forceps and clean gloves. The sampling devices, containers and the filtration system were cleaned according to GEOTRACES protocols (Cutter et al., 2010).

Particulate organic carbon and nitrogen (POC and pN) samples were collected using the *CCGS Amundsen* rosette, consisting of 24×12 L Niskin bottles, a Sea-Bird SBE 911 CTD, and fluorometer, transmissometer, colored dissolved organic matter and oxygen sensors. POC and pN samples were collected at the same stations (excepting station CAA9) and depths where particulate trace elements were sampled. On-board the ship, between two to nine liters of seawater were filtered through $0.7\ \mu\text{m} / 25\ \text{mm}$ pre-combusted (450°C for 4 h) glass fiber (GF) filters (Whatman), which were later stored at -20°C (Brown et al., 2014).

3.2. Sample processing and analysis

In order to prevent contamination, the processing and analysis of particulate trace elements was conducted at the University of British Columbia (UBC) in class 1000 laboratories, pressurized with HEPA filtered air, and under class 100 laminar flow fume hoods. All the plasticware used during the sample preparation and analysis were cleaned according to GEOTRACES protocols (Cutter et al., 2010).

3.2.1. Particulate trace elements

Filters containing the particulate fraction were digested at UBC following the protocol described by Ohnemus et al. (2014). In brief, the organic fraction and the Supor filter matrix were dissolved by reflux heating with sulfuric acid and hydrogen peroxide ($\text{H}_2\text{SO}_4/\text{H}_2\text{O}_2$), followed by mineral matrix dissolution by reflux heating using a mixture of mineral acids (HNO_3 , hydrochloric acid [HCl] and hydrofluoric acid [HF]). After the digestion procedure, the clear residues were resuspended in 1% HNO_3 with 10 ppb of indium as an internal standard; particulate samples were diluted prior to ICP-MS analysis (the particulate digestion protocol is fully described in the [supporting information](#): Supplementary methods). All reagents used in the digestion and subsequent sample preparation (H_2SO_4 , HNO_3 , HCl, HF and H_2O_2) were Optima grade (Fisher Scientific, Ontario, Canada).

Particulate Al, V, Fe, Mn and P were analyzed from a twelve-point calibration curve prepared in 1% trace metal grade HNO_3 from 1 ppm certified single element standards. The analyses were conducted by a high resolution Thermo Finnigan Element2 ICP-MS in the Pacific Centre for Isotopic and Geochemical Research (PCIGR), an analytical center at UBC. A medium mass resolution was selected for Fe, V and Mn in order to remove isobaric interferences, and Al and P were analyzed using low mass resolution. During sample analysis, solution blanks (1% HNO_3 Milli-q water with indium) and filter blanks were run to ensure quality throughout the measurements; particulate trace element concentrations reported here were corrected for the analytical blank by subtracting the average solution blank on the corresponding analytical day and from the filter blank measurements. The accuracy and precision of this

method was tested by analyzing the certified reference material BCR-414, and GEOTRACES inter-calibration samples collected in the Pacific Ocean. The BCR-414, as well as GEOTRACES inter-calibration samples underwent the same digestion and analytical method used to analyze the Canadian Arctic GEOTRACES samples. Results from these analyses (mean, standard deviation and relative standard deviation values) as well as, solution and filter blank concentrations are listed in Table S1. Measured values in this study are in good agreement with consensus values, yielding recoveries ranging from 76 to 123% ($104 \pm 11\%$) for Al, V, Fe, Mn and P (Table S1).

3.2.2. Particulate organic carbon and particulate nitrogen (POC and pN)

Frozen filters containing POC and pN were oven dried at 60 °C for 24 h at UBC, and then acid fumed with concentrated HCl for three days and dried at 50 °C for 24 h to remove particulate inorganic carbon (Brown et al., 2014). POC and pN analyses were conducted by the use of a carbon/nitrogen/sulfur vario MICRO cube analyzer (Elementar), and the concentrations reported here were corrected by subtracting the average concentrations of pre-combusted blank GF filters. The detection limits of the analyses – 3σ of replicate measurement of pre-combusted blank GF filters – were 0.012 mg for POC ($n = 10$) and 0.009 mg for pN ($n = 8$).

3.3. Tidal stress estimates, particle tracking simulations and statistical analysis

Tidal flow over topography can generate strong sediment resuspension events. In order to identify the spatial distribution and the prevalence of these events in Baffin Bay and the Labrador Sea, we mapped tidal stress, calculated by squaring the barotropic tidal speeds (Wang, 2002). The magnitude of the tidal stress is proportional to the integrated effect of resuspension on an area, i.e. high tidal stress suggests frequent resuspension events (Wang, 2002). The barotropic tidal speeds were extracted from the MOG2D-G hydrodynamic gravity waves model (Carrère and Lyard, 2003) by Epstein (2018).

The paths of the winter Bering Sea water (wBSW) sampled at the three Canada Basin stations were traced from August 2015 backward two years using Ocean Parcels (Lange and Seville, 2017) with 5-day averaged velocity fields from a 1/12 degree coupled ocean-ice model of the Arctic and Northern Hemispheric Atlantic (Hu et al., 2018) configuration of the Nucleus for European Modeling of the Ocean (NEMO; Madec et al., 2017). In order to trace the wBSW, water parcels were released at model depth levels 23–30 (i.e. 110–380 m).

Python 3.6.0. programming language and NumPy, Matplotlib, SciPy and pandas libraries were used for statistical analysis and graphic design. Particulate trace element data, as well as POC and pN, are presented as mean \pm standard deviation (otherwise noted), and differences between concentration means have been tested using student t-test at a significance level of 5% or lower. A linear least-squares regression fit (slope, intercept, correlation coefficient and

p-value) has been applied to evaluate the relationship among different trace elements.

4. RESULTS

4.1. Dataset overview

This study presents total pAl, pV, pFe, pMn, pP, POC and pN distribution in the Canadian Arctic Ocean (CAO), across three deep basins: The Canada Basin, Baffin Bay and the Labrador Sea, as well as pP, POC and pN distributions in the shallow Canadian Arctic Archipelago. These are the first observations collected in the CAO for many of these elements (full dataset presented in this manuscript is included in the Research Data Electronic Annex).

Among the deep CAO basins, the Canada Basin (CB) and the Labrador Sea (LS) had low concentrations of lithogenic-derived particulate elements, such as pAl, pFe and pV (albeit pV surface and subsurface distributions are not associated with lithogenic phases; discussed below), while the concentrations of these elements were higher in Baffin Bay (BB; Table S2 and Fig. 2). However, even for BB, lithogenic particle concentrations in the deep (~ 1000 – 3500 m) basins were significantly lower than those measured in the shallow and shelf-dominated Canadian Arctic Archipelago (CAA; Table S2 and Fig. 2).

The concentrations of pP, POC and pN in the Canadian Arctic Ocean did not follow the trends described above for lithogenic elements. Concentrations of these biogenic-derived elements were similar across the CAA, BB and LS, while significantly (p -value < 0.05) lower values were observed in the CB (Table S2 and Fig. 2). The highest values of lithogenic particulate elements (Fig. 2, red points) were commonly associated with near bottom waters, while biogenic-derived elements (pP, POC and pN) peak at the surface. The distribution of particulate Mn, unlike the other elements, was similar across the CB, CAA and BB, whereas much lower concentrations were measured in the LS (Table S2 and Fig. 2).

4.2. Vertical distributions of particulate elements in the Canadian Arctic Ocean

4.2.1. Particulate Al, V, Fe and Mn

The Canada Basin: Surface ($\sigma_\theta < 24$ and $z < 40$ m) concentrations of pAl, pV, pFe and pMn slowly decreased with depth down to the top of the winter Bering Sea Water halocline layer (wBSW), where concentrations increased with depth, especially for pV and pMn. At the shelf-break CB2 station, a steady increase of pAl, pV and pFe was observed with depth below the halocline assembly. This increase contrasts with the low and relatively uniform values measured across the Atlantic Layer (AL = FSB + BSB) and Canada Basin Deep Waters (CBDW) at CB3 (Fig. 3). Particulate trace metal concentrations in the AL and CBDW at CB4 were significantly higher (p -value < 0.001) than those of CB3. Particulate Mn profiles resembled those of pAl, pV and pFe for surface and subsurface waters, but, unlike the previous elements, no differences were found among the three stations below the halocline assembly (Fig. 3).

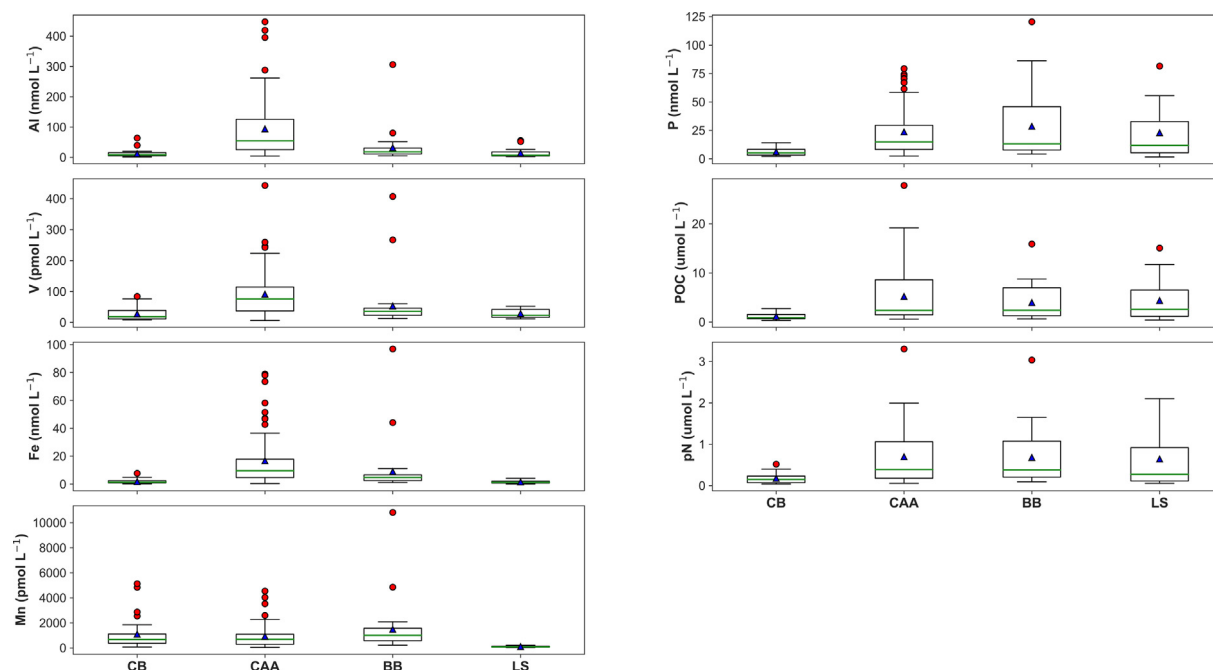


Fig. 2. Observed concentration ranges of particulate trace elements (pAl, pV, pFe, pMn and pP) and particulate organic carbon and particulate nitrogen (POC and pN) in the Canada Basin (CB), Baffin Bay (BB) and the Labrador Sea (LS). Particulate Al, V, Fe and Mn data in the Canadian Arctic Archipelago (CAA) were retrieved from Colombo et al. (2021). Boxes mark the 25th and 75th percentiles for all data points, whisker bars represent 10th and 90th percentiles, solid green horizontal lines in each box represent the median, blue triangles represent average values, and red points are the outliers representing data that extend beyond the whiskers.

Baffin Bay: Similar to CB, particulate concentrations in BB surface waters ($\sigma_\theta < 26.3$) were uniformly low. This low signature extended down to the top of the Arctic Water (AW), where a subsurface peak was observed, reaching concentrations as high as 34.2 nmol L^{-1} , 57.3 pmol L^{-1} , 7.12 nmol L^{-1} , 2084 pmol L^{-1} for pAl, pV, pFe and pMn, respectively (Fig. 3). Underneath the AW, vertical distributions of pAl, pV and pFe across the West Greenland Intermediate Waters (WGIW) and Baffin Bay Deep Waters (BBDW) exhibited distinct spatial differences. The lowest concentrations of these elements were measured at station BB2, followed by BB3 and BB1 (Fig. 3). Clear maxima of pAl, pV and pFe were observed in the deepest samples, close to the sea-floor, where concentrations were two to ten-fold higher than WGIW and BBDW values (Fig. 3). For pMn, this spatial difference in deep water (WGIW + BBDW) distributions among BB stations was not as clear as that described for pAl, pV and pFe ($\text{BB1} > \text{BB3} > \text{BB2}$), albeit two to ten-fold higher maximum concentrations were also found in the deepest samples (Fig. 3).

The Labrador Sea: The concentrations of pAl, pFe and pMn in surface waters ($\sigma_\theta < 27.4$) were lower than those measured in BB, but in the same range as the CB values, with the exception of high surface pV ($45.7 \pm 6.43 \text{ pmol L}^{-1}$), and the rather high pAl measured at 9 m depth (55.4 nmol L^{-1} ; Fig. 3). Interestingly, subsurface and deep water pFe and pMn concentrations at station LS2 were considerably higher than at K1, which was not the case for pAl (Fig. 3). At LS2 station, from ~ 300 to 500 m , a subsurface peak with

concentrations as high as pAl: 20.4 nmol L^{-1} , pV: 17.5 pmol L^{-1} , pFe: 3.29 nmol L^{-1} , pMn: 182 pmol L^{-1} was present. Particulate concentrations increased from the base of Labrador Sea Waters-2015 (LSW-2015) towards the sea floor, with the highest values found at the base of the Northeast Atlantic Deep Water (NSDW; Fig. 3). At station K1, a shallower subsurface peak of pAl was observed from approximately $100\text{--}150 \text{ m}$, while pAl deep water concentrations remained nearly uniform across LSW-2015, LSW-87/94 and NSDW, with much higher concentrations (7-fold higher than LSW and NSDW) in the Denmark Strait Overflow Water (DSOW). Similarly, pFe and pMn did not change significantly across LSW and NSDW, but a sharp increase in their concentrations was measured in DSOW (\sim two-fold higher than LSW and NSDW; Fig. 3).

Despite the spatial variability across the deep CAO basins, as a general trend, pAl and pV concentrations from CB, BB and LS, not accounting for benthic nepheloid layers, are higher than those reported for the East Pacific Zonal transect (GP16), the South Atlantic Ocean (GA06_w), the Eastern Tropical Atlantic Ocean (GA06_w) and the North Atlantic (GA01_e; Fitzsimmons et al., 2017; Milne et al., 2017; Gourain et al., 2019; GEOTRACES Intermediate Data Product Group, 2021). Similarly, pMn concentrations in CB and BB are considerably higher than those of aforementioned basins ($\sim 100\text{--}300 \text{ pmol kg}^{-1}$), while LS concentrations fall within the range of reported values for other major basins. For pFe, CAO concentrations are within the same range as those reported for the South Atlantic Ocean, the Eastern Tropical

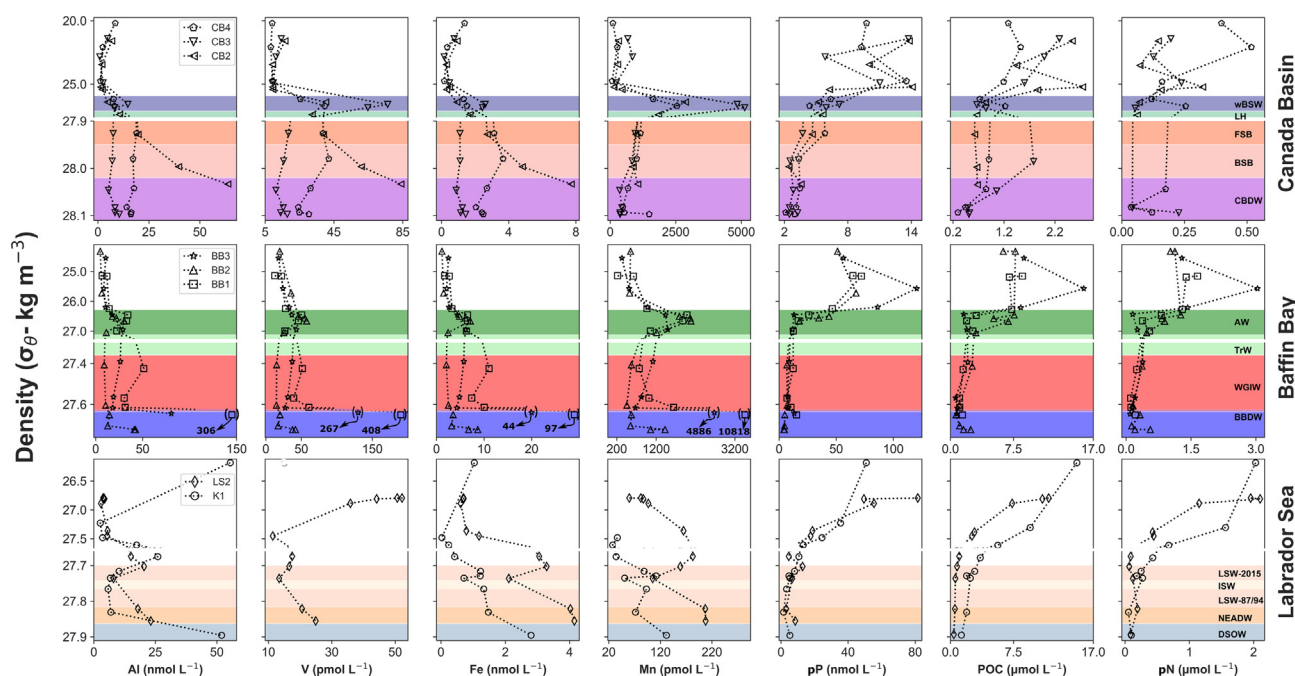


Fig. 3. Profiles of particulate Al, V, Fe, Mn, pP, POC, pN versus potential density (σ_θ) for the deep stations in the Canada Basin (upper panel: CB2–CB4), Baffin Bay (middle panel: BB1–BB3) and the Labrador Sea (lower panel: LS2 and K1). As the deepest samples from Baffin Bay had extremely high concentrations of Al, V, Fe and Mn, these values are shown between parentheses to emphasize the features of the rest of the profile. Colored bands label important water masses to facilitate the interpretation and discussion of the trace element data following Aksenov et al. (2011), Kondo et al. (2016), Tang et al. (2004), Curry et al. (2011), Yashayaev and Loder (2009 and 2016). wBSW: winter Bering Sea Water ($\sigma_\theta = 25.9\text{--}27.1$ and $z = \sim 100\text{--}300$ m), LH: Lower Halocline, FSB: Fram Strait Branch, BSB: Barents Sea Branch (FSB + BSB: $\sigma_\theta = 27.9\text{--}28.0$ and $z = \sim 350\text{--}1200$ m), CBDW: Canada Basin Deep Water ($\sigma_\theta > 28.1$ and $z > 1200$ m), AW: Arctic Water ($\sigma_\theta = 26.3\text{--}27.1$ and $z = \sim 40\text{--}180$ m), TrW: transitional water ($\sim 180\text{--}300$ m), WGIW: West Greenland Intermediate Water ($\sigma_\theta = 27.3\text{--}27.6$ and $z = \sim 300\text{--}800$ m), BBDW: Baffin Bay Deep Water ($\sigma_\theta > 27.6$ and $z > 800$ m), LSW: Labrador Sea Water ($\sigma_\theta = 27.70\text{--}27.81$; LS2: $\sim 470\text{--}1870$ m and K1: $\sim 140\text{--}2060$ m), ISW: Icelandic Slope Water, NSDW: Northeast Atlantic Deep Water ($\sigma_\theta = 27.81\text{--}27.86$; LS2: $\sim 1870\text{--}2400$ m and K1: $\sim 2060\text{--}2640$ m), DSOW: Denmark Strait Overflow Water ($\sigma_\theta > 27.86$; LS2: > 2400 and K1: > 2640 m).

Atlantic Ocean and the North Atlantic ($\sim 0.5\text{--}5$ nmol kg^{-1}), but higher than pFe measured in the East Pacific Zonal transect (< 1 nmol kg^{-1}), where particulate trace metal concentrations are generally low (Fitzsimmons et al., 2017; Milne et al., 2017; Gourain et al., 2019; GEOTRACES Intermediate Data Product Group, 2021).

4.2.2. Particulate phosphate (pP), organic carbon (POC) and nitrogen (pN)

The Canada Basin: The lowest pP, POC and pN concentrations of this study were measured in this basin; these elements peaked at the surface ($z = \sim 10$) and subsurface ($\sigma_\theta = 24.8\text{--}25.2$ and $z = 60\text{--}70$ m; Fig. 3), where transmissivity diminished and chlorophyll-a (Chl-a) was highest (Figure S2). Below 100 m ($\sigma_\theta = \sim 25.7\text{--}26.1$), pP, POC and pN decreased with depth, although the difference in concentrations between surface and deep waters was not as large as that observed in the CAA, BB and LS (Figs. 3 and 4).

Baffin Bay: pP, POC and pN were highest in the upper 40 m ($\sigma_\theta < 26.3$), with concentrations ranging from 43.7 to 72.1 nmol L^{-1} , 6.29 to 8.57 $\mu\text{mol L}^{-1}$ and 1.02 to 1.65 $\mu\text{mol L}^{-1}$, respectively, at BB1 and BB2, and highest at BB3 (pP: 120 nmol L^{-1} , POC: 15.9 $\mu\text{mol L}^{-1}$, pN:

3.04 $\mu\text{mol L}^{-1}$; Fig. 3). Across AW, POC and pN concentrations were lowest at station BB3, followed by BB1 and BB2 (Fig. 3), where a deeper subsurface Chl-a peak and transmissivity drop were recorded (Figure S2). Underneath AW, pP, POC and pN continued to decline with depth through the WGIW (Fig. 3).

The Labrador Sea: pP, POC and pN were elevated in surface waters ($z < 40$ m) and sharply decreased from the subsurface waters to the top of LSW-2015 (Fig. 3). Underneath LSW-2015, pP, POC and pN concentrations steadily decreased with depth to the DSOW, where minima in POC and pN concentrations were reached.

The Canadian Arctic Archipelago: As described for the deep basins, pP, POC and pN were highest in surface waters, while much lower concentrations were measured in deeper waters ($\sigma_\theta = \sim 26.3\text{--}26.8$ and $z > 100$ m). Marked differences in the distributions of these elements were noticed in the CAA, with considerably lower concentrations measured in the western CAA (CB1 and CAA8 stations) compared to eastern CAA regions (CAA1–CAA7 and CAA9; Fig. 4). Surface concentrations of pP, POC and pN in the western CAA ranged between 8.08 to 25.3 nmol L^{-1} , 1.95 to 3.33 $\mu\text{mol L}^{-1}$ and 0.109 to 0.425 $\mu\text{mol L}^{-1}$, respectively (Fig. 4). On the other hand,

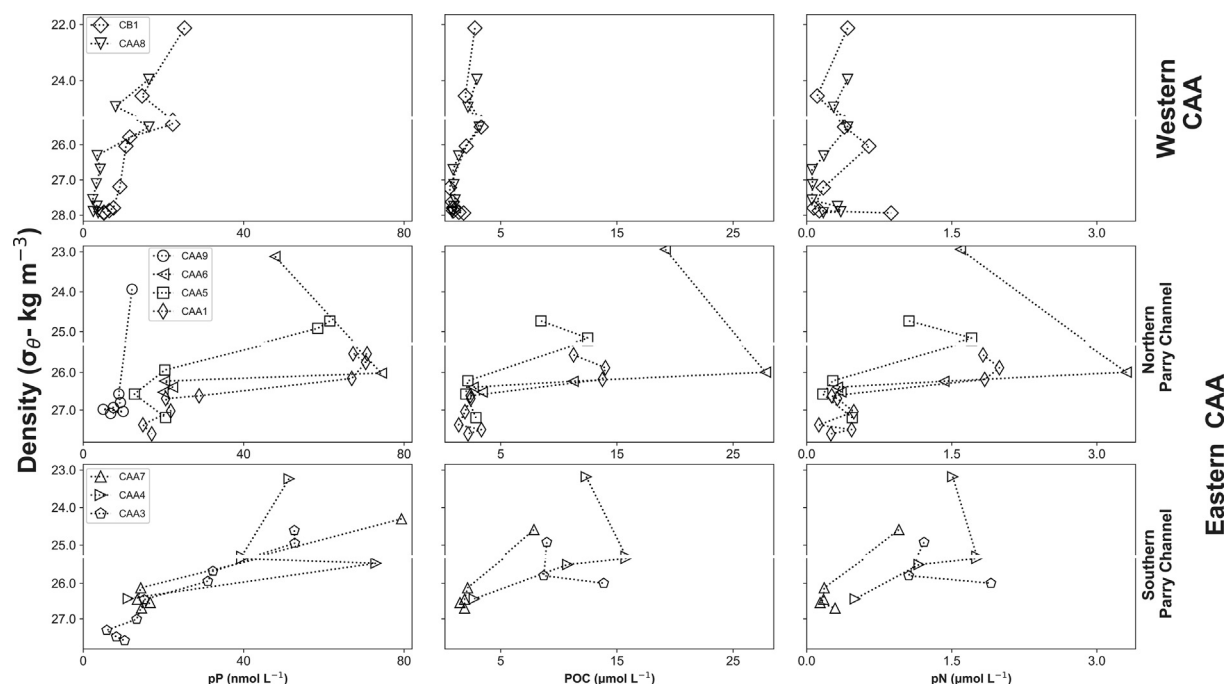


Fig. 4. Profiles of pP, POC and pN versus potential density (σ_θ) in the Canadian Arctic Archipelago (CAA). Note that the vertical axis scales vary.

in the eastern CAA, surface and subsurface concentrations were higher (pP: 31.1–74.9 nmol L⁻¹, POC: 7.86–27.78 μ mol L⁻¹, pN: 0.953–3.304 μ mol L⁻¹), and decreased uniformly to the bottom (Fig. 4).

5. DISCUSSION

5.1. the importance of advective transport, nepheloid layers and authigenic Mn oxides in modulating the distributions of lithogenic elements and Mn

In order to elucidate the sources and dominant phases (i.e. lithogenic, biogenic, authigenic) of particulate samples in the Canadian Arctic Ocean (CAO), we normalized our data to pAl, and compared elemental pAl ratios to average upper continental crustal ratios (UCC; Shaw et al., 2008; Rudnick and Gao, 2013). Particulate Al has been extensively used as a lithogenic tracer due to its high natural abundance in the earth's crust, its similar concentration range in both the UCC and bulk continental crust (the relatively constant ratio of metal to aluminum in crustal rocks) and its scarce anthropogenic sources (Covelli and Fontolan, 1997; Ohnemus and Lam, 2015; Lam et al., 2018; Lee et al., 2018; Gourain et al., 2019).

In the CB, BB and LS, particulate concentrations show three distinctive patterns. On one hand, pV and pFe were strongly positively correlated with pAl across many orders of magnitude ($R^2 = 0.83$ and 0.90 , respectively), and their ratios were in agreement with those reported for the UCC (Fig. 5, upper panel), reflecting the dominance of lithogenic-derived inputs of these elements. On the other hand, pP was instead correlated with POC and pN (section 5.2) and decoupled from pAl ($R^2 = 0.01$), with ratios that

strongly deviated from the UCC (Fig. 5), which evidence the dominant role of biogenic sources (i.e. phytoplankton biomass). And last, unlike the aforementioned particulate elements, pMn display only a moderate correlation with pAl ($R^2 = 0.60$; Fig. 5, upper panel), with distributions that vary greatly in the lithogenic fraction (from 1 to 100%; Fig. 5, lower panel). These results suggest that distinct particle inputs and/or alteration processes modulate pMn in the deep CAO basins.

No significant correlations ($R^2 < 0.01$ and p -value > 0.05) were found between pAl, pV, pFe and pMn versus pP, which indicate that inputs from phytoplankton do not contribute substantially to variations in these particulate elements across the CAO. Therefore, the biogenic fraction of pFe – the most abundant trace metal in phytoplankton (Ho et al., 2003) – is completely masked by its lithogenic input (Fig. 5).

5.1.1. The influence of lateral advection of shelf-derived waters and Mn oxide formation on surface and subsurface particulate distributions in the CB, BB and the LS

Due to the high latitude and remote location of the CAO, atmospheric fluxes tend to be attenuated in this region (Marsay et al., 2018; Shelley et al., 2018). This fact likely explains the relatively low surface concentrations measured in CB, BB and LS (Fig. 3), far away from shelf areas where freshwater and landfast ice are important sources of particulate elements (Giesbrecht et al., 2013; Kondo et al., 2016; Gourain et al., 2019). Lithogenic inputs dominate the concentrations of pAl and pFe ($>90\%$) in surface waters across the entire CAO (Fig. 5). Among the deep water basins, the highest pAl and pFe concentrations were measured in BB surface waters (Fig. 3), which captures the

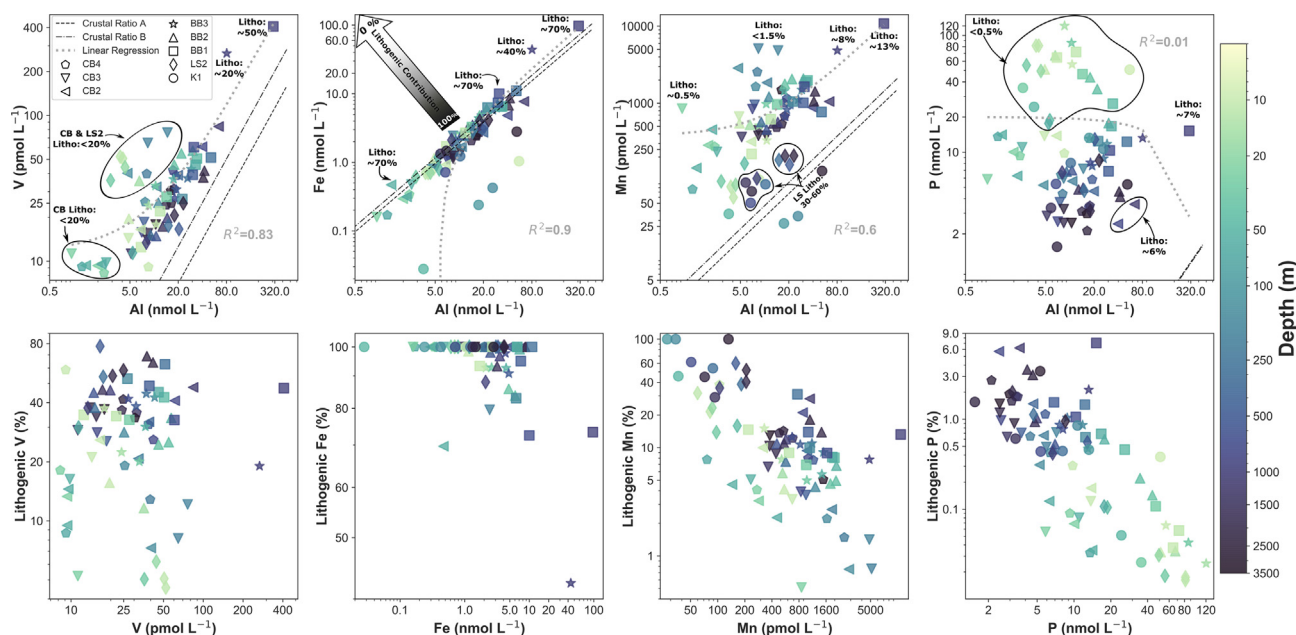


Fig. 5. Upper panels: relationship between pV, pFe, pMn and pP versus pAl in the Canada Basin (CB), Baffin Bay (BB) and the Labrador Sea (LS); note the logarithmic scale of the plots. The depth of the samples is indicated with the color scale; data are from all deep basin stations and all depths. Linear regression lines and R^2 values are displayed in the figure (light gray), as well as average upper continental crustal (UCC) ratios for these elements indicated by the dashed and dash-dotted black lines. UCC particulate elements to Al molar ratios are selected from Shaw et al. (2008), who reported continental surface Precambrian shield composition in Canada (crustal ratio A), and from an updated continental crust composition review (crustal ratio B; Rudnick and Gao 2013). Additionally, the lithogenic fraction (%) of some samples is annotated in the figure to illustrate differential sources for these elements. Samples plotting along the crustal ratios are assumed to be lithogenically derived (lithogenic contribution arrow). Lower panels: lithogenic fractions (%) of pV, pFe, pMn and pP calculated as $\%pTE_{litho} = 100 \times \left(\frac{pAl}{pTE} \right)_{sample} \times \left(\frac{pTE}{pAl} \right)_{UCC}$, where pTE is the lithogenic fraction of a given particulate trace element, and the UCC are the upper continental crust ratios retrieved from Rudnick and Gao (2013), as this work presented the most updated review of the continental crust composition.

CAA outflow enriched in pAl and pFe (Colombo et al., 2021). In the CB, the downwelling Beaufort Gyre entrains and accumulates freshwater and sea ice (Proshutinsky et al., 2009). These freshwater inputs, and its associated lithogenic particulate load (Measures, 1999; Giesbrecht et al., 2013), to CB surface waters ($S = 25.1$ – 29.2 ; Figure S1) are expected to drive the higher pAl and pFe values found at the shallowest depths (200 to 400% higher) compared with underlying waters (Fig. 3).

On the other hand, the lithogenic contribution of pV and pMn in CAO surface waters represents less than 40 and 30% of bulk concentrations. Elevated non-lithogenic contributions of pMn and pV could be linked to enhanced primary production at the surface, which increases the export of biogenic-derived particles (Twining et al., 2015; Lee et al., 2018; Gourain et al., 2019; Whitmore et al., 2019). Nonetheless, strong phytoplankton production of pMn (essential micronutrient) in surface waters is not supported by our dataset given that non-lithogenic pMn fractions do not change significantly across CB and BB (Figs. 3 and 5), despite the large differences in the biological productivity observed among these two deep basins (CB - Chl-a \ll BB Chl-a; Figs. S2, S3 and S4). Indeed, the lowest pMn concentrations were measured in LS (Fig. 3), where intense phytoplankton spring blooms took place

(Figs. S3 and S4). Moreover, pMn distributions in the CAO did not follow the trends of pP, POC and pN, whose spatial and vertical distributions are strongly controlled by phytoplankton productivity (section 5.2). Hence, the excess of pMn over UCC values are likely explained by authigenic formation of $Mn^{+3/4}$ oxides, most probably bacterially-mediated Mn^{+2} oxidation/precipitation. Even though the abiotic oxidation of Mn is thermodynamically favored under typical pH and pO_2 conditions in most oceanic waters, this reaction has an extremely low kinetic rate. Bacteria are known to accelerate Mn^{+2} oxidation, and therefore are considered the most important drivers of Mn precipitation in aquatic environments (Cowen and Silver, 1984; Cowen and Bruland, 1985; Sunda and Huntsman, 1988; Moffett, 1997; Lam and Bishop, 2008; Yigiterhan et al., 2011; Noble et al., 2013; Lee et al., 2018; Wright et al., 2018; Morton et al., 2019). Surface pMn concentrations in the CAO are lowest in the upper water column, despite being largely dominated by non-lithogenic sources (~ 70 – 95% ; Figs. 3 and 6). This low surface pMn concentrations may reflect diminished bacterial Mn oxidizing activity (photoinhibition) and photoreduction of Mn oxides (Mn^{+3}) by sunlight, resulting in lower rates of particulate Mn formation in surface waters (Sunda and Huntsman, 1988, 1990; Francis et al., 2001). Particulate V cycling in CAO

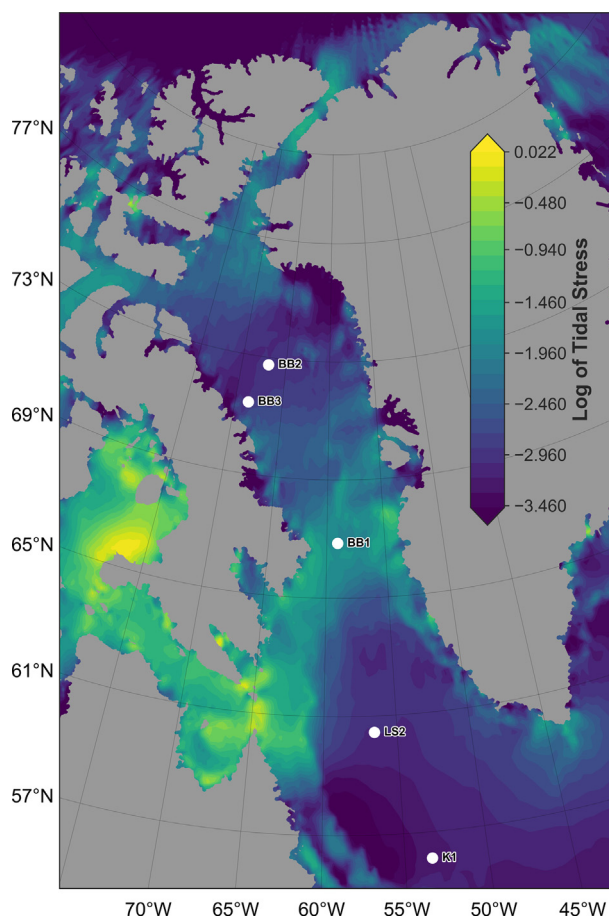


Fig. 6. Tidal stress, a proxy for the integrated effect of sediment resuspension (Methods, section 3.3). Barotropic tidal speeds were extracted from a hydrodynamic gravity waves model (Carrère and Lyard, 2003) by Epstein (2018).

surface waters is tightly coupled with pMn, as dissolved V (dV) has proven to be easily scavenged onto Mn oxide particles (Whitmore et al., 2019 and references therein). The unexpectedly high pV in surface LS waters (45.7 ± 6.43 p mol L⁻¹ and Litho_pV < 7%; ~100–200% higher than CB and BB surface concentrations; Fig. 3) where the lowest pMn concentrations were measured, could be attributed to the stripping of dV by the increased particle flux (Whitmore et al., 2019) associated with the aforementioned phytoplankton bloom (Figs. S2, S3 and S4).

Beneath surface waters, pAl and pFe concentrations rapidly increase within the winter Bering Sea Water (wBSW) in CB and the Arctic Water (AW) in BB (Fig. 3). These subsurface waters are advected from the shallow and shelf-dominated Chukchi Sea and CAA, respectively, carrying a unique biogeochemical signature to the deep basins. The wBSW is distinguished by a weak temperature minimum, high nutrient concentrations, high dissolved nutrient-like trace metals, high colored dissolved organic matter (CDOM), and low oxygen concentrations (Hioki et al., 2014; Kondo et al., 2016; Colombo et al., 2020; Figs. S1 and S2). These properties show the signature of the large organic matter remineralization and sedimentary denitrification (low N* values) that occurs over the

Bering and Chukchi shelves (Hioki et al., 2014; Granger et al., 2018). The fresh CAA outflow into Baffin Bay is also characterized by a temperature minimum, high dissolved nutrient-like trace metals, high CDOM, and relatively high oxygen concentrations, resulting from the intense mixing and sediment resuspension in the CAA (Colombo et al., 2020, 2021; Figs. S1 and S2). The elevated values of pAl and pFe in both wBSW in CB and AW in BB are attributed to advective transport of lithogenic-derived particles (Litho_pFe: ~80–100 %; Fig. 5) from the shallow Chukchi and CAA shelves, where the incorporation of resuspended sediment into shelf waters has been recently reported (Xiang and Lam, 2020; Colombo et al., 2021). The sediment-rich wBSW in CB and AW in BB cascade down-slope, and are then transported long distances along their flow paths (e.g. > 1400 km from CAA3 and CAA4 in the southern Lancaster Sound, via BB3 on the Baffin Bay slope and out to BB1 in the Davis Strait).

In contrast, the much sharper subsurface pMn peak in CB and BB is dominated by the non-lithogenic fraction (wBSW: > 97 % and AW: > 90 %, respectively; Figs. 3 and 5). Distinctively high Mn oxide concentration, many times higher than those found in other oceanographic regions, was also described by Xiang and Lam (2020) in

halocline waters in the Chukchi Abyssal Plain, the Makarov Basin and western Canada Basin. Here, we demonstrate that this Mn oxide signature is still prevalent in the Beaufort Sea (CB stations), and in BB (Fig. 3). The pMn peak in wBSW and AW is hypothesized to be produced within the water column (bacterially-mediated Mn oxide precipitation), rather than being an advected sedimentary signature (reduction in the sediment → diffusion to the overlying water → oxidation → precipitation of redox sensitive elements such as Fe and Mn).

In the Chukchi Sea, where large pulses of organic matter trigger strong reducing conditions in sediments, large fluxes of dissolved manganese (Mn^{+2}) are generated in porewater and diffused into the overlying seawater (Granger et al., 2018; Vieira et al., 2019; Xiang and Lam, 2020). Given its slow oxidation kinetics and the potential photoinhibition of Mn oxidizing bacteria in the shallow Chukchi shelves (<50 m), most of Mn^{+2} remains in the dissolved phase for a long time in the halocline waters (wBSW) – leaving Chukchi shelf waters depleted of pMn oxides and highly enriched in dMn (Xiang and Lam, 2020), which are transported to the slope region where Mn authigenically re-precipitates.

In the CAA, characterized by reduced pulses of organic matter and strong mixing regimes, the reductive benthic supply of Mn^{+2} and its subsequent precipitation is not anticipated to be significant, and the dominance of Mn oxides in the CAA is related to the advection of wBSW from the CB (Colombo et al., 2021). The strongly reduced authigenic sedimentary formation of Mn oxides in the Chukchi Sea and CAA, and the ubiquity of non-lithogenic pMn across the entire water column in CAO (with the exception of LS), suggest that pMn in wBSW and in AW is a result of increased oxidative Mn precipitation in the water column, as described for other basins (Sunda and Huntsman, 1988; Yigiterhan et al., 2011; Noble et al., 2013; Morton et al., 2019). In effect, the pMn peak in both wBSW in CB and AW in BB is associated with a rapid decrease with depth in dMn concentrations in these basins, where the pMn fraction transitions from less than 20% of total Mn (dMn + pMn) in surface waters (dMn is dominant) to ~55–70% in wBSW and AW (Figs. S5 and S6).

Marine microbial communities, including Mn oxidizing bacteria, are widely distributed in ocean waters, however, their abundance and diversity vary both spatially and vertically based on environmental conditions (e.g. light penetration, temperature, availability of labile organic matter, nutrients and micronutrients such as Fe and Mn; Dick et al., 2006; Zakharova et al., 2010; Zinger et al., 2011). Both, the wBSW and AW have the potential to sustain large populations of Mn oxidizing bacteria given their distinctive environmental conditions. These water masses are relatively deep – where sunlight, and therefore, microbial photoinhibition is attenuated – and have elevated concentrations of dissolved Mn and Fe, advected from the shallow Chukchi and CAA shelves, which would allow Mn oxidizing bacteria to proliferate (Sunda and Huntsman, 1988; Moffett, 1997; Zakharova et al., 2010; Colombo et al., 2020). Another feature that wBSW and AW have in common is their close interaction with the seafloor upstream while they transit shallow shelf environments (Chukchi

Sea and the CAA). As result of the interaction with the seafloor, where microbe communities are taxonomically richer and more abundant than in the water column (Feng et al., 2009; Zinger et al., 2011), wBSW and AW are not only enriched in lithogenic particles (as evidenced by pAl and pFe distributions) and CDOM, but they also could potentially entrain sedimentary microbes (Walsh et al., 2016). An analogous process has been described for hydrothermal plumes, which entrain manganese oxidizing bacteria from surficial sediments and transport them long distances; resulting in high rates of bacterially-mediated Mn^{+2} oxidation within these plumes (Dick et al., 2006, 2013; Fitzsimmons et al., 2017).

We posit two complementary mechanisms which could be driving the sharp non-lithogenic pMn peak in wBSW in the CB interior: 1) advective transport of small Mn oxides particles precipitated over the Chukchi shelf-break and/or slope region 2) enhanced precipitation/concentration effect of dMn supplied from above. Strong bacterially-mediated oxidation occurs in the water column over the shallow Chukchi shelf-break, where the high dMn signature (~40–200 nmol kg⁻¹) is rapidly lost (Kondo et al., 2016; Vieira et al., 2019; Jensen et al., 2020). Once the wBSW is advected to the ocean interior, dMn concentrations are further diminished over the Chukchi slope, dropping to 1.34 ± 0.57 nM about 350 km away from Chukchi shelf (Kondo et al., 2016). Beyond the slope towards the CB interior, dMn is conserved, as the dMn concentrations measured in the CB interior (1.37 ± 0.41 nmol kg⁻¹; Colombo et al., 2020) are nearly the same as those measured ~350 km offshore Chukchi Sea. The rapid loss of dMn over the slope and the bacterially-mediated Mn oxide precipitation is reflected in the sediment record. The near-shore shallow sediments within the Chukchi shelves, contain low and lithogenic derived Mn, whereas in the slope region, the sediments are greatly enriched in non-lithogenic Mn (Macdonald and Gobeil, 2012). Although most of the non-lithogenic Mn particulates originating in the shelf-break and/or slope region are rapidly lost due to sinking, the smaller sized Mn oxides could be entrained and transported long distances to the CB interior. Small microbially catalyzed pMn oxides (Cowen and Silver, 1984; Cowen and Bruland, 1985) have been shown to be transported long distances (4000 km at 0.2–0.5 cm s⁻¹) from hydrothermal vent sources (Fitzsimmons et al., 2017). In addition, no significant pMn settling across isopycnals was observed in the distal hydrothermal plume due to the small (0.5–1 µm) and low density nature of Mn oxide coatings on bacterial cells (Fitzsimmons et al., 2017; González-Santana et al., 2020). The Stokesian settling velocities of pure birnessite (major manganese-bearing mineral; density = 2900 kg m⁻³) particles with 0.5 to 1 µm diameters are 4–17 m y⁻¹, however, these values are likely reduced if we account for the lower specific gravity of bacterial-Mn oxide capsule complexes. Results from Ocean Parcels particle track simulations (Methods, section 3.3) suggest that it takes from about one to three years for the wBSW to travel from the Chukchi shelves to our sampled stations (CB2: 580 km at 1.8 cm s⁻¹, CB3: 896 km at 2.8 cm s⁻¹, CB4: 410 km at 1.3 cm s⁻¹; speeds are an

average estimate based on the distance the parcels travelled in a given time period within Ocean Parcels). Given the timescale of wBSW circulation in the CB, and even considering the sinking rates of pure birnessite, advective transport of small-size pMn from the Chukchi shelf-break is a plausible mechanism explaining the wBSW pMn peaks observed in the CB.

Enhanced oxidative precipitation of the Mn flux (pMn + dMn) falling through the water column could be a complementary mechanism. Ice-rafted sediments likely supply a significant Mn flux to the Canada Basin upper ocean (Measures, 1999; Rogalla et al., 2021). Because of the fast reversible oxidation / reduction cycling of Mn, with timescale of a couple of weeks (oxidation rate 0.06 per day and reduction rate 0.04 per day; Bruland et al., 1994; Rogalla et al., 2021), Mn is cycled back and forth between the dissolved and oxidized pools multiple times once it is sourced from surface waters. While Mn is in its oxidized phase, particles will sink at rates governed by their density and size, thus generating a downward flux. This Mn flux is then entrained in wBSW, where Mn oxidizing bacteria populations are potentially abundant and Mn oxidation rates may be greater. The lighter and smaller bacterially-mediated Mn oxides (Fitzsimmons et al., 2017) that are formed in the wBSW barely sink (Stokesian settling velocities for 0.5–1 μm particles $< 17 \text{ m y}^{-1}$), and thus, would be concentrated in this water mass. These two mechanisms described above are also expected to take place in AW in the BB, where sharp non-lithogenic pMn peaks were observed in this study.

The pV maxima in wBSW and AW have relatively high non-lithogenic contributions (~ 70 – 92 and ~ 55 – 75 %, respectively; Figs. 3 and 6), attributed to the scavenging of dV onto the abundant authigenic Mn oxides present in these subsurface waters. A similar pV peak in CB around the 26.6 kg m^{-3} isopycnal surface (wBSW) was reported by Whitmore et al. (2019), who argued that the strong dV removal and the subsequent pV enrichment is largely controlled by the adsorption of dV onto Mn oxides, strong scavengers of many trace elements, in deep basins.

In the LS, lithogenic inputs govern the subsurface distribution of pAl and pFe (100 %), as well as those of pV (~ 54 – 78 %) and pMn (~ 38 – 60 %), compared to CB and BB where authigenic Mn oxides exert a dominant role shaping pV and pMn subsurface distributions (Fig. 5). The diminished influence of pMn oxides in the LS could be explained by micronutrient limitation (such as dissolved Mn or Fe) of Mn oxidizing bacteria in this region (Moffett, 1997). Indeed, the LS yielded the lowest subsurface concentrations of these metals, while considerably higher concentrations were measured in wBSW and AW in CB and BB, respectively (Colombo et al., 2020), and/or the relative isolation of LS from continental margins with regards to CB and BB. Further research, such as bioassay/incubation experiments, genomic measurements and taxonomic identification, is required to unravel the authigenic Mn cycling in CB and BB, and the notable reduction of authigenic Mn formation in LS.

5.1.2. Boundary transport of resuspended sediments and near-bottom enrichment of pTE

The Arctic Circumpolar Boundary Current (ACBC; $\sigma_\theta > 27.9$ and $z > 350 \text{ m}$) is anticipated to modulate the distributions of pAl, pV and pFe in CB, causing higher concentrations of these elements at CB2 station, followed by CB4 and CB3 (Fig. 3). The main ACBC components, the Fram Strait Branch (FSB) and Barents Sea Branch (BSB), travel around the rim of the Arctic Ocean (Fig. 1), mobilizing sediment particles from the continental margin, and advecting these particle-rich waters to the Canada Basin interior (Aksenov et al., 2011; Aguilar-Islas et al., 2013; Giesbrecht et al., 2013; Kondo et al., 2016; Xiang and Lam, 2020). As a result of their locations, both CB2 and CB4 are more directly impacted by FSB and BSB cyclonic circulation than CB3 station. This difference is notably reflected in substantially contrasting concentrations of pAl, pV and pFe in open ocean CB stations ($\text{CB4} \gg \text{CB3}$), and much higher concentrations observed at the shelf-break CB2 station, where transmissivity values were lowest (Figs. 1, 3 and S2). The relative isolation of CB3 station from the ACBC and enhanced advective transport of dissolved Fe and Mn to CB4 has been recently documented (Grenier et al., 2019; Colombo et al., 2020). Here we show that mid-depth lateral transport from continental margins also exerts a strong control over pAl, pV and pFe distributions, and possibly other lithogenic-derived elements. Preferential sinking of larger particles, with faster settling velocities than smaller ones, likely explains the high concentrations of pAl, pV and pFe observed close to the shelf-break and slope stations and their reduction along the flow path, as reported in studies where size-fractionated data were available (Lam et al., 2015, 2018; Lee et al., 2018; Xiang and Lam, 2020).

The vertical distributions of pAl, pV and pFe are also strongly influenced by advective transport of resuspended sediments from continental margins in the WGIW in BB (Fig. 1). The highest concentrations of pAl, pV and pFe were measured in Davis Strait (BB1), where the tidal stresses are the highest of BB (~ 0.016 – $0.069 \text{ m}^2 \text{ s}^{-2}$; Figs. 3 and 6). These high concentrations are likely associated with the resuspension of sediments in this region where intense cyclonic boundary currents have been recorded (Tang et al., 2004). In contrast, pAl, pV and pFe were uniformly low at station BB2 (Fig. 3), which is located in the center of Baffin Bay (Fig. 1), largely isolated from the cyclonic circulation of WGIW (Colombo et al., 2019b). Station BB2 has also low tidal stresses, suggesting reduced prevalence of sediment resuspension (tidal stress $< 0.0009 \text{ m}^2 \text{ s}^{-2}$; Fig. 6). Vertical distributions of pMn in CB and BB, in contrast to pAl, pV and pFe, were similar among sampled stations, despite the disparate influence of advective transport of resuspended particles from continental margins in both basins (Fig. 3). This distinctive behavior is linked to the relatively low lithogenic contributions of pMn (~ 5 – 30 %; Figs. 3 and 6) in FSB, BSB and WGIW waters, which contrasts with those of pV and pFe (~ 30 – 70 and > 90 %, respectively).

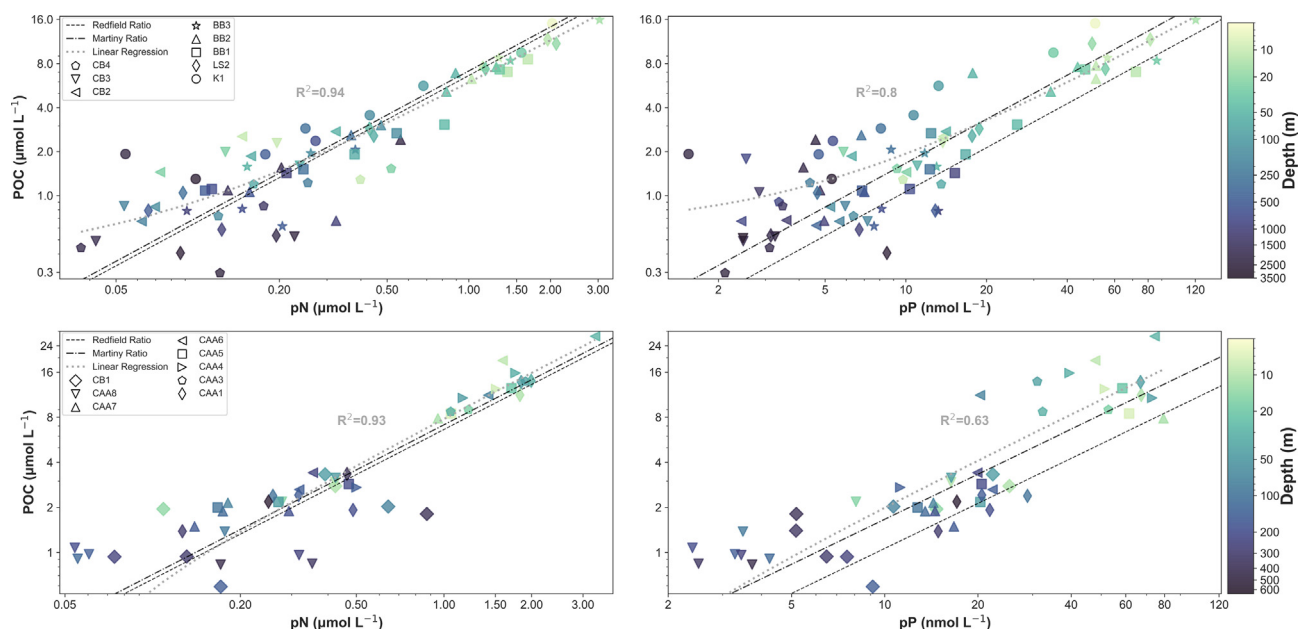


Fig. 7. Relationship between POC versus pN and pP in deep basins (upper panels) including the Canada Basin (CB), Baffin Bay (BB) and the Labrador Sea (LS and K1), and in the shallow Canadian Arctic Archipelago (lower panels; CAA). Note the logarithmic scale of the plots. The depth of the samples is indicated with the color scale; data are from all 16 stations and all depths. Linear regression lines and R^2 values are displayed in the figure (light gray), as well as Redfield and Martiny POC:pN (6.6 and 7.2) and POC:pP (106 and 167) stoichiometric ratios indicated by the dashed and dash dotted black lines (Martiny et al., 2013).

Distributions of particulate Al, V, and Fe in Labrador Sea deep waters (LSW, NSDW and DSOW) are predominantly controlled by lithogenic sources (Litho_pV: ~55–77 and Litho_pFe: > 90%). Their concentrations are relatively low and similar to those measured in the isolated central stations in CB and BB (CB3 and BB2; Fig. 3), which reveals reduced lateral transport of these elements from continental slope regions. Compared to CB and BB deep waters, pMn has its lowest concentrations (Fig. 3), and the strongest lithogenic contribution (~30–100%; Fig. 5) in LSW, NSDW and DSOW, presumably related to diminished Mn oxidizing activity in LS as discussed in Section 5.1.1.

Near-bottom enrichment of particulate metals is a widespread feature in deep basins, usually related to the interactions of deep currents with bottom topography (sediment resuspension) and/or to redox cycling within and above the sediment, as reported in numerous studies (Gourain et al., 2019; Hansel, 2017; Jeandel et al., 2015; Lam et al., 2015, 2018; Lam and Bishop, 2008; Ohnemus and Lam, 2015; Vieira et al., 2019). In this study, pAl, pV, pFe and pMn spiked in the deepest samples in CB (CB2 and CB4), BB (BB1–BB3) and LS (LS2 and K1), with concentrations considerably higher than those measured in overlying waters (Fig. 3). At the Baffin Bay stations located along the slope (BB3) and Davis Strait (BB1), the bottom samples are highly enriched in particulate elements, and have pTE: pAl ratios largely exceeding those of UCC and relatively low lithogenic fractions (Litho_pV: 20 and 47%, Litho_pFe: 42 and 73%, Litho_pMn: 8 and 13%, for BB3 and BB1 respectively; Figs. 3 and 5). The relatively low lithogenic fraction of pFe is particularly notable as its dis-

tribution is dominated by lithogenic sources (close to 100%) in the vast majority of the analyzed samples (Fig. 5, lower panel). This evidence shows that redox mobilization of reduced Mn and Fe species and their subsequent precipitation is an important source of pFe and pMn for the deepest samples at BB1 and BB3. This signal is superimposed to that of the resuspension of lithogenic particles as demonstrated by a spike in pAl. At station BB2 in central Baffin Bay, the presence of authigenic Mn (redox-mobilized) differs from the lithogenic prevalence of pV and pFe (Litho_pV: 64%, Litho_pFe: 100%, Litho_pMn: 13%). This difference is likely related to lower productivity and organic matter inputs in central Baffin Bay compared to shelf regions (Wyatt et al., 2013; Figs. S2 and S3) and/or increased organic matter remineralization in the water column at the deeper BB2 station (BB1 & BB2: 1000 m vs. BB2 > 2000 m). These environmental conditions would in turn presumably decrease reducing conditions in the sediments at BB2 station, yielding a redox potential appropriate for Mn reduction, but higher than that required for Fe reduction. In LS, where particulate concentrations rapidly increased towards near-bottom waters (Fig. 3), the deepest samples have pTE:pAl ratios similar to those of UCC and greater lithogenic contributions (Litho_pV: 60%, Litho_pFe: 100 and 100%, Litho_pMn: 52 and 100% for LS2 and K1 respectively; Fig. 5). The flow of deep water boundary currents (NSDW and DSOW) over bottom topography in LS (Fig. 1) is expected to cause intense sediment resuspension events (Middag et al., 2015), as suggested by the sharp decrease of dissolved trace elements that are particle reactive, such as dissolved Pb and ^{230}Th at LS2 and K1 stations below 2500 m (Grenier et al.,

2018; Colombo et al., 2019b), and consequently results in elevated lithogenic-derived particulate elements (Fig. 3). This energetic boundary current in LS, and associated sediment resuspension events, probably diminishes reductive sedimentary processes, thereby explaining the lower contribution of authigenic pMn oxides to bottom LS waters, as suggested by Ohnemus and Lam (2015).

5.2. Biogenic-derived elements: pP, POC and pN dynamics across the productivity gradients of the Canadian Arctic Ocean

In the Canadian Arctic Ocean (CAO), particulate phosphorous (pP) as well as particulate organic carbon and nitrogen (POC and pN) were elevated in the upper 100 m, where Chl-a peaked and transmissivity dropped, indicating the dominant role of biological production in modulating vertical distributions of these elements (Figs. 3–5). In contrast, below ~100 m, the predominance of organic matter regeneration is reflected in a rapid decrease of pP, POC and pN with depth, with concentrations remaining uniformly low in deep waters (Figs. 3 and 5). The spatial distributions of these elements revealed notable differences between CB and the rest of the CAO, with extremely low pP, POC and pN in CB, similar to those reported by Trimble and Baskaran (2005) and Brown et al. (2014), in contrast to those observed in CAA, BB and LS (Fig. 2). These differences are linked to the low Chl-a (Figs. S2, S3 and S4), primary productivity and export production rates in CB compared to the much higher values in the rest of CAO (Hill et al., 2013; Varela et al., 2013; Wyatt et al., 2013; Crawford et al., 2015; Lehmann et al., 2019; Xiang and Lam, 2020). The low levels of primary productivity in CB result from both light and nitrate limitation (Tremblay et al., 2008; Tremblay and Gagnon, 2009), which could be further limited by dissolved Fe availability in the summertime (during phytoplankton blooms) as described by Taylor et al. (2013).

Within the CAA, pP, POC and pN also display a spatial contrast between western and eastern CAA regions, with lower concentrations measured from M'Clure Strait to Viscount Melville Sound (stations CB1 and CAA8) versus those from Barrow Strait and Lancaster Sound (Fig. 4). It should be noted that the stations CB1 and CAA8 in western CAA were sampled in early and late September, whereas eastern stations were sampled in early August, potentially affecting the distribution of pP, POC and pN due to the seasonal solar irradiance variation (Michel et al., 2015). However, the spatial differences in pP, POC and pN distributions in the CAA observed in this study are consistent with the variability in phytoplankton communities and regimes identified by Ardyna et al. (2011). The Beaufort Sea and the western CAA are characterized by an oligotrophic flagellate-based system which transitions to an eutrophic diatom-based system in eastern CAA (Lancaster Sound). Therefore, an interplay of multiple environmental processes affecting light and nutrient availability may explain the above noted spatial differences in this shallow environment. Sea ice pervasiveness (limiting solar irradiation), increased stratification (hindering nutrient

replenishment from bottom waters), and reduced availability of micronutrients (e.g. Fe) in the western CAA, contrast with the longer ice-free season and enhanced mixing, sediment resuspension and micronutrient availability of the eastern CAA (Michel et al., 2006, 2015; Ardyna et al., 2011; Hughes et al., 2017; Colombo et al., 2021). The distributions and concentrations of pP, POC and pN in the CAO, and in the CAA in particular, agree with previous studies in the Arctic region (Trimble and Baskaran, 2005; Wyatt et al., 2013; Brown et al., 2014), and correlate with primary production patterns (Chl-a) retrieved from both satellite data and in-situ measurements during the Canadian Arctic GEOTRACES cruise (CB and western CAA << eastern CAA, BB and LS; Figs. 3 and S2–S4).

The particulate C:N:P ratios from all particulate samples collected during the Canadian Arctic GEOTRACES cruise show strong POC:pN and POC:pP relationships in the deep basins ($R^2 = 0.94$ and 0.80 , respectively) and the shallow CAA ($R^2 = 0.93$ and 0.63 , respectively, Fig. 7). Although C:N:P ratios are known to be influenced by phytoplankton community composition, and hence, regional differences exist, our data compare well with the canonical Redfield ratio (106:16:1) and with recent global elemental phytoplankton composition estimates (166.6:23.4:1; Martiny et al., 2013; Fig. 7). Within the euphotic zone, POC:pN and POC:pP ratios agree more closely with Redfield and Martiny ratios and the lithogenic contributions to pP are negligible, whereas the deeper samples (>100 m) are more dispersed, deviating from phytoplankton ratios, and have slightly higher lithogenic contributions to pP (Figs. 5 and 8). In the upper 100 m of BB and LS, the most productive basins in the CAO, particulate C:N ratios (6.3 ± 1.3) closely reflect phytoplankton stoichiometries (6.6–7.1; Martiny et al., 2013), while in the CAA these ratios are somewhat higher (8.4 ± 2.6). This is most probably related to enhanced terrigenous-derived organic matter inputs with higher C:N ratios (Dittmar and Kattner, 2003) in this land-dominated environment where shelf-water interactions and freshwater inputs are increased (Colombo et al., 2021). In the upper 100 m of CB, however, particulate C:N ratios are very scattered and deviate from Redfield and Martiny ratios, with lower ratios at CB4 (3.0–7.4) and much higher ratios at CB2 and CB3 stations (6.7–19.9). A similarly high POC:pN ratio (17.9) is observed in the upper 50 m at the entrance of M'Clure Strait (station CB1). Past studies have described the large spatial variability in particulate C:N ratios in the CAO. While, extremely low ratios (2.1–3.5) in central CB are associated with low concentrations of phytoplankton carbon and larger contribution of small flagellates, higher ratios (>10) are observed in shelf waters, which are potentially related to the influence of freshwater inputs (riverine, glacial, and/or sea ice meltwater) of allochthonous carbon detritus (Brown et al., 2014; Crawford et al., 2015; Fragoso et al., 2017). Lastly, compared with phytoplankton stoichiometry, the consistently higher POC:pP ratios of the deepest samples in CB, BB and LS, as well as in M'Clure Strait (Fig. 7), may reflect the preferential remineralization of P relative to C in sinking particulate matter (Faul et al., 2005).

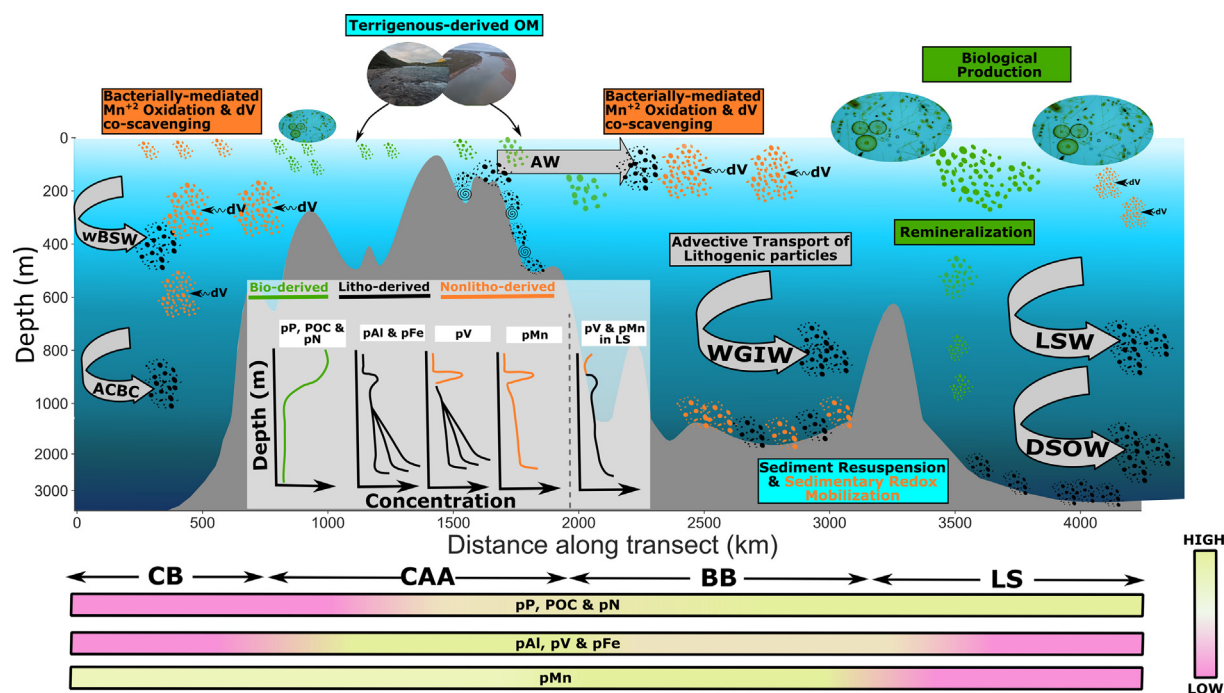


Fig. 8. Conceptual scheme of the dominant phases (biogenic, lithogenic and non-lithogenic) and key processes controlling the distributions of particulate Al, V, Fe, Mn, P as well as particulate organic carbon and nitrogen (POC and pN) across the Canadian Arctic Ocean (CAO). CB: Canada Basin, CAA: Canadian Arctic Archipelago, BB: Baffin Bay, LS: Labrador Sea, wBSW: winter Bering Sea Water, ACBC: Arctic Circumpolar Boundary Current, AW: Arctic Water, WGIW: West Greenland Intermediate Water, LSW: Labrador Sea Water, DSOW: Denmark Strait Overflow Water. The size of the label fonts and symbols represent the relative abundance of particulate trace element and the importance of the described processes.

6. CONCLUSIONS

The present study investigates the processes which control the biogeochemical cycling of particulate elements (Al, V, Fe, Mn, P, POC and pN) in the Canadian Arctic Ocean (CAO) deep basins, as well as pP, POC and pN in the shallow Canadian Arctic Archipelago (CAA). A combination of both lithogenic sources and enhanced scavenging onto Mn oxides appears to shape pV distribution in surface and subsurface waters (Fig. 8). Particulate Al, Fe and V have identical deep water profiles ($z > 300$ m), revealing the importance of lateral transport of resuspended sediments from shelf/slope regions. The Canada Basin (CB), Baffin Bay (BB) and the Labrador Sea (LS) are all characterized by strong deep water boundary currents (ACBC, WGIW, NEADW and DSOW), which flow along shelf and slope regions, become enriched in resuspended particles, and transport this signature offshore into the basins (Fig. 8). Indeed, the stations sampled along the flow path of the boundary currents have higher concentrations of pAl, pFe and pV than those located in the central basins. The distributions of particulate Mn, in contrast, are governed by water column Mn²⁺ oxidation, showing maximum concentrations between ~ 100 and 300 m across the CB and

BB, presumably related to strengthened activity of Mn-oxidizing bacteria – fueled by excess of dissolved Mn inputs advected from shallow shelves – and photoinhibition relief in subsurface waters (Fig. 8). The occurrence of Mn oxides (non-lithogenic component) is greatly reduced in the LS, where the lithogenic sources dominate bulk particulate distributions of Al, Fe, V, and also Mn, despite the low concentrations measured in this basin, distant from continental margins. Benthic nepheloid layers are also abundant in the CAO, where above mentioned particulate elements are enriched in the deepest samples due to sediment resuspension and/or redox mobilization (Fig. 8). The distributions and cycling of pP, POC and pN are tightly linked to the strong productivity gradient present in the CAO, with the lowest values registered in the oligotrophic CB, progressively increasing their concentrations towards the shallow CAA, BB and the LS, where large phytoplankton blooms have been registered. Accordingly, the C:N:P stoichiometry in the upper 100 m closely reflects that of phytoplankton, although higher C:N ratios have been observed in the land-dominated CAA where terrigenous-derived inputs are likely increased. In the deep water column (>100 m), where remineralization is prevalent, C:N:P ratios deviate from canonical ratios (Fig. 8).

Declaration of Competing Interest

The authors declare that they have no known competing financial interests or personal relationships that could have appeared to influence the work reported in this paper.

ACKNOWLEDGEMENTS

This work was supported by the Natural Sciences and Engineering Research Council of Canada (Grant NSERC-CCAR) and the Northern Scientific Training Program. We thank the captain and crew of the CCGS Amundsen as well as Chief Scientist Roger Francois and the science crew of the Canadian Arctic GEOTRACES program for their assistance in sample collection. We also thank ArcticNet; Jean-Eric Tremblay's group for providing the nutrient data for the Canadian GEOTRACES 2015 cruise. The University of British Columbia PCGIR and its staff are thanked for assistance with sample analyses. Data collected during these cruises are made available by the ArcticNet science program, which is supported by the Canada Foundation for Innovation and NSERC.

RESEARCH DATA

The particulate Arctic data reported in this study is available in the Research Data document (Electronic Annex).

APPENDIX A. SUPPLEMENTARY DATA

Supplementary data to this article can be found online at <https://doi.org/10.1016/j.gca.2022.02.013>.

REFERENCES

- Aguilar-Islas A. M., Rember R., Nishino S., Kikuchi T. and Itoh M. (2013) Partitioning and lateral transport of iron to the Canada Basin. *Polar Sci.* **7**, 82–99.
- Aksenov Y., Ivanov V. V., Nurser A. J. G., Bacon S., Polyakov I. V., Coward A. C., Naveira-Garabato A. C. and Beszczynska-Moeller A. (2011) The arctic circumpolar boundary current. *J. Geophys. Res. Ocean.* **116**, 1–28.
- Anderson R., Mawji E., Cutter G., Measures C. and Jeandel C. (2014) GEOTRACES: Changing the Way We Explore Ocean Chemistry. *Oceanography* **27**, 50–61.
- Ardyna M., Gosselin M., Michel C., Poulin M. and Tremblay J.-É. (2011) Environmental forcing of phytoplankton community structure and function in the Canadian High arctic: Contrasting oligotrophic and eutrophic regions. *Mar. Ecol. Prog. Ser.* **442**, 37–57.
- Beszczynska-Möller A., Woodgate R., Lee C., Melling H. and Karcher M. (2011) A Synthesis of Exchanges Through the Main Oceanic Gateways to the Arctic Ocean. *Oceanography* **24**, 82–99.
- Brown K. A., McLaughlin F. A., Tortell P. D., Varela D. E., Yamamoto-Kawai M., Hunt B. and François R. (2014) Determination of particulate organic carbon sources to the surface mixed layer of the Canada Basin, Arctic Ocean. *J. Geophys. Res. Ocean.* **119**, 1084–1102.
- Bruland K. W., Orians K. J. and Cowen J. P. (1994) Reactive trace metals in the stratified central North Pacific. *Geochim. Cosmochim. Acta* **58**, 3171–3182.
- Carrère L. and Lyard F. (2003) Modeling the barotropic response of the global ocean to atmospheric wind and pressure forcing - Comparisons with observations. *Geophys. Res. Lett.* **30**, 1275–1279.
- Charette M. A., Lam P. J., Lohan M. C., Kwon E. Y., Hatje V., Jeandel C., Shiller A. M., Cutter G. A., Thomas A., Boyd P. W., Homoky W. B., Milne A., Thomas H., Andersson P. S., Porcelli D., Tanaka T., Geibert W., Dehairs F. and Garcia-Orellana J. (2016) Coastal ocean and shelf-sea biogeochemical cycling of trace elements and isotopes: Lessons learned from GEOTRACES. *Philos. Trans. R. Soc. A Math. Phys. Eng. Sci.*, 374.
- Cheize M., Planquette H. F., Fitzsimmons J. N., Pelletier E., Sherrell R. M., Lambert C., Bucciarelli E., Sarthou G., Le Goff M., Liorzou C., Chéron S., Viollier E. and Gayet N. (2019) Contribution of resuspended sedimentary particles to dissolved iron and manganese in the ocean: An experimental study. *Chem. Geol.* **511**, 389–415.
- Cid A. P., Nakatsuka S. and Sohrin Y. (2012) Stoichiometry among bioactive trace metals in the Chukchi and Beaufort Seas. *J. Oceanogr.* **68**, 985–1001.
- Colombo M., Brown K. A., De Vera J., Bergquist B. A. and Orians K. J. (2019a) Trace metal geochemistry of remote rivers in the Canadian Arctic Archipelago. *Chem. Geol.* **525**, 479–491.
- Colombo M., Jackson S. L., Cullen J. T. and Orians K. J. (2020) Dissolved iron and manganese in the Canadian Arctic Ocean: on the biogeochemical processes controlling their distributions. *Geochim. Cosmochim. Acta* **277**, 150–174.
- Colombo M., Rogalla B., Li J., Allen S. E., Orians K. J. and Maldonado M. T. (2021) Canadian Arctic Archipelago shelf-ocean interactions: a major iron source to Pacific derived waters transiting to the Atlantic. *Global Biogeochem. Cycles* **35**, 1–17.
- Colombo M., Rogalla B., Myers P. G., Allen S. E. and Orians K. J. (2019b) Tracing Dissolved Lead Sources in the Canadian Arctic: Insights from the Canadian GEOTRACES Program. *ACS Earth Sp. Chem.* **3**, 1302–1314.
- Covelli S. and Fontolan G. (1997) Application of a normalization procedure in determining regional geochemical baselines. *Environ. Geol.* **30**, 34–45.
- Cowen J. P. and Bruland K. W. (1985) Metal deposits associated with bacteria: implications for Fe and Mn marine biogeochemistry. *Deep Sea Res. Part A Oceanogr. Res. Pap.* **32**, 253–272.
- Cowen J. P. and Silver M. W. (1984) The association of iron and manganese with bacteria on marine macroparticulate material. *Science (80-)* **224**, 1340–1342.
- Crawford D. W., Wyatt S. N., Wrohan I. A., Cefarelli A. O., Giesbrecht K. E., Kelly B. and Varela D. E. (2015) Low particulate carbon to nitrogen ratios in marine surface waters of the Arctic. *Global Biogeochem. Cycles* **29**, 2021–2033.
- Cuny J., Rhines P. B. and Kwok R. (2005) Davis Strait volume, freshwater and heat fluxes. *Deep Res. Part I Oceanogr. Res. Pap.* **52**, 519–542.
- Cuny J., Rhines P. B., Niiler P. P. and Bacon S. (2002) Labrador Sea Boundary Currents and the Fate of the Irminger Sea Water. *J. Phys. Oceanogr.* **32**, 627–647.
- Curry B., Lee C. M. and Petrie B. (2011) Volume, Freshwater, and Heat Fluxes through Davis Strait, 2004–05*. *J. Phys. Oceanogr.* **41**, 429–436.
- Cutter G. R., Andersson P., Codispoti L., Croot P., Francois R., Lohan M. C., Obata H., van der Loeff M., François R., Lohan M. C., Obata H., Rutgers v. d., Loeff M., Francois R., Lohan M. C., Obata H., and van der Loeff M. (2010) *Sampling and Sample-handling Protocols for GEOTRACES Cruises*. Available

- at: <http://www.geotraces.org/library/geotraces-policies/170-sampling-and-sample-handling-protocols-for-geotraces-cruises>.
- Dick G. J., Anantharaman K., Baker B. J., Li M., Reed D. C. and Sheik C. S. (2013) The microbiology of deep-sea hydrothermal vent plumes: Ecological and biogeographic linkages to seafloor and water column habitats. *Front. Microbiol.* **4**, 1–16.
- Dick G. J., Lee Y. E. and Tebo B. M. (2006) Manganese(II)-oxidizing *Bacillus* spores in Guaymas basin hydrothermal sediments and plumes. *Appl. Environ. Microbiol.* **72**, 3184–3190.
- Dittmar T. and Kattner G. (2003) The biogeochemistry of the river and shelf ecosystem of the Arctic Ocean: a review. *Mar. Chem.* **83**, 103–120.
- Epstein J.-L. (2018) *The impact of internal tide mixing parameterizations in an eddy-permitting model of the Arctic Ocean*. University of British Columbia.
- Faul K. L., Paytan A. and Delaney M. L. (2005) Phosphorus distribution in sinking oceanic particulate matter. *Mar. Chem.* **97**, 307–333.
- Feng B. W., Li X. R., Wang J. H., Hu Z. Y., Meng H., Xiang L. Y. and Quan Z. X. (2009) Bacterial diversity of water and sediment in the Changjiang estuary and coastal area of the East China Sea. *FEMS Microbiol. Ecol.* **70**, 236–248.
- Fischer J., Schott F. A. and Dengler M. (2004) Boundary Circulation at the Exit of the Labrador Sea. *J. Phys. Oceanogr.* **34**, 1548–1570.
- Fitzsimmons J. N., John S. G., Marsay C. M., Hoffman C. L., Nicholas S. L., Toner B. M., German C. R. and Sherrell R. M. (2017) Iron persistence in a distal hydrothermal plume supported by dissolved-particulate exchange. *Nat. Geosci.* **10**, 195–201.
- Fragoso G. M., Poulton A. J., Yashayaev I. M., Head E. J. H. and Purdie D. A. (2017) Spring phytoplankton communities of the Labrador Sea (2005–2014): Pigment signatures, photophysiology and elemental ratios. *Biogeosciences* **14**, 1235–1259.
- Francis C. A., Co E. M. and Tebo B. M. (2001) Enzymatic Manganese(II) Oxidation by a Marine α -Proteobacterium. *Appl. Environ. Microbiol.* **67**, 4024–4029.
- GEOTRACES Intermediate Data Product Group (2021) The GEOTRACES Intermediate Data Product 2021 (IDP2021).
- Giesbrecht T., Sim N., Orians K. J. and Cullen J. T. (2013) The distribution of dissolved and total dissolvable aluminum in the Beaufort sea and Canada basin region of the Arctic Ocean. *J. Geophys. Res. Ocean.* **118**, 6824–6837.
- González-Santana D., Planquette H., Cheize M., Whitby H., Gourain A., Holmes T., Guyader V., Cathalot C., Pelleter E., Fouquet Y. and Sarthou G. (2020) Processes Driving Iron and Manganese Dispersal From the TAG Hydrothermal Plume (Mid-Atlantic Ridge): Results From a GEOTRACES Process Study. *Front. Mar. Sci.* **7**, 1–17.
- Gourain A., Planquette H., Cheize M., Lemaitre N., Menzel B. J. and L., Shelley R., Lherminier P. and Planquette H. (2019) Inputs and processes affecting the distribution of particulate iron in the North Atlantic along the GEOVIDE (GEOTRACES GA01) section. *Biogeosciences* **16**, 1563–1582.
- Granger J., Sigman D. M., Gagnon J., Tremblay J.-É. and Mucci A. (2018) On the properties of the Arctic Halocline and deep water masses of the Canada Basin from nitrate isotope ratios. *J. Geophys. Res. Ocean.* **123**, 1–16.
- Grenier M., François R., Soon M., Baconnais I., Pham V. and Jeandel C. (2018) Ocean circulation and land-ocean exchanges off the north eastern Canadian coasts as told by dissolved geochemical tracers. In *Goldschmidt Abstracts* p. 2018 880.
- Grenier M., François R., Soon M., Rutgers van der Loeff M., Yu X., Valk O., Not C., Moran S. B., Edwards R. L., Lu Y., Lepore K. and Allen S. E. (2019) Changes in Circulation and Particle Scavenging in the Amerasian Basin of the Arctic Ocean over the Last Three Decades Inferred from the Water Column Distribution of Geochemical Tracers. *J. Geophys. Res. Ocean.* **124**, 9338–9363.
- Hansel C. M. (2017) Manganese in Marine Microbiology. In *Advances in Microbial Physiology*. Elsevier Ltd., pp. 37–83.
- Hill V. J., Matrai P. A., Olson E., Suttles S., Steele M., Codispoti L. A. and Zimmerman R. C. (2013) Synthesis of integrated primary production in the Arctic Ocean: II. In situ and remotely sensed estimates. *Prog. Oceanogr.* **110**, 107–125.
- Hioki N., Kuma K., Morita Y., Sasayama R., Ooki A., Kondo Y., Obata H., Nishioka J., Yamashita Y., Nishino S., Kikuchi T. and Aoyama M. (2014) Laterally spreading iron, humic-like dissolved organic matter and nutrients in cold, dense subsurface water of the Arctic Ocean. *Sci. Rep.* **4**, 1–9.
- Ho T. Y., Finkel Z. and V, Milligan A. J., Wyman K., Falkowski P. G. and Morel F. M. M. (2003) The elemental composition of some marine phytoplankton. *J. Phycol.* **39**, 1145–1159.
- Homoky W. B., Weber T., Berelson W. M., Conway T. M., Henderson G. M., van Hulten M., Jeandel C., Severmann S. and Tagliabue A. (2016) Quantifying trace element and isotope fluxes at the ocean-sediment boundary: A review. *Philos. Trans. R Soc. A Math. Phys. Eng. Sci.* **374**, 1–43.
- Hu X., Sun J., On C. T. and Myers P. G. (2018) Thermodynamic and dynamic ice thickness contributions in the Canadian Arctic Archipelago in NEMO-LIM2 numerical simulations. *Cryosphere* **12**, 1233–1247.
- Hughes K. G., Klymak J. M., Hu X. and Myers P. G. (2017) Water mass modification and mixing rates in a $1/12^\circ$ simulation of the Canadian Arctic Archipelago. *J. Geophys. Res. Ocean.* **122**, 803–820.
- Jackson J. M., Allen S. E., Carmack E. C. and McLaughlin F. A. (2010) Suspended particles in the Canada Basin from optical and bottle data, 2003–2008. *Ocean Sci.* **6**, 799–813.
- Jeandel C. (2016) Overview of the mechanisms that could explain the “Boundary Exchange” at the land-ocean contact. *Philos. Trans. R. Soc. A Math. Phys. Eng. Sci.*, 374.
- Jeandel C. and Oelkers E. H. (2015) The influence of terrigenous particulate material dissolution on ocean chemistry and global element cycles. *Chem. Geol.* **395**, 50–66.
- Jeandel C., Peucker-Ehrenbrink B., Jones M., Pearce C., Oelkers E. H., Godderis Y., Lacan F., Aumont O. and Arsouze T. (2011) Ocean margins: The missing term in oceanic element budgets? *Eos (Washington, DC)* **92** 217.
- Jeandel C., Rutgers van der Loeff M., Lam P. J., Roy-Barman M., Sherrell R. M., Kretschmer S., German C. and Dehairs F. (2015) What did we learn about ocean particle dynamics in the GEOSECS-JGOFS era? *Prog. Oceanogr.* **133**, 6–16.
- Jensen L. T., Morton P., Twining B. S., Heller M. I., Hatta M., Measures C. I., John S., Zhang R., Pinedo-Gonzalez P., Sherrell R. M. and Fitzsimmons J. N. (2020) A comparison of marine Fe and Mn cycling: U.S. GEOTRACES GN01 Western Arctic case study. *Geochim. Cosmochim. Acta* **288**, 138–160.
- Kondo Y., Obata H., Hioki N., Ooki A., Nishino S., Kikuchi T. and Kuma K. (2016) Transport of trace metals (Mn, Fe, Ni, Zn and Cd) in the western Arctic Ocean (Chukchi Sea and Canada Basin) in late summer 2012. *Deep Sea Res. Part I Oceanogr. Res. Pap.* **116**, 236–252.
- Lam P. J. and Bishop J. K. B. (2008) The continental margin is a key source of iron to the HNLC North Pacific Ocean. *Geophys. Res. Lett.* **35**, 1–5.
- Lam P. J., Lee J. M., Heller M. I., Mehic S., Xiang Y. and Bates N. R. (2018) Size-fractionated distributions of suspended particle concentration and major phase composition from the U.S. GEOTRACES Eastern Pacific Zonal Transect (GP16). *Mar. Chem.* **201**, 90–107.

- Lam P. J., Ohnemus D. C. and Auro M. E. (2015) Size-fractionated major particle composition and concentrations from the US GEOTRACES North Atlantic Zonal Transect. *Deep-Sea Res. Part II: Top. Stud. Oceanogr.* **116**, 303–320.
- Lange M. and Seville E. V. (2017) Parcels v0. 9: prototyping a Lagrangian ocean analysis framework for the petascale age. *Geosci. Model Dev.* **10**, 4175–4186.
- Lee J. M., Heller M. I. and Lam P. J. (2018) Size distribution of particulate trace elements in the U.S. GEOTRACES Eastern Pacific Zonal Transect (GP16). *Mar. Chem.* **201**, 108–123.
- Lehmann N., Kienast M., Granger J., Bourbonnais A., Altabet M. A. and Tremblay J.-É. (2019) Remote Western Arctic Nutrients Fuel Remineralization in Deep Baffin Bay. *Global Biogeochem. Cycles* **2018GB006134**.
- Lozier M. S., Bacon S., Bower A. S., Cunningham S. A., De Jong M. F., De Steur L., De Young B., Fischer J., Gary S. F., Greenan B. J. W., Heimbach P., Holliday N. P., Houpt L., Inall M. E., Johns W. E., Johnson H. L., Karstensen J., Li F., Lin X., Mackay N., Marshall D. P., Mercier H., Myers P. G., Pickart R. S., Pillar H. R., Straneo F., Thierry V., Weller R. A., Williams R. G., Wilson C., Yang J., Zhao J. and Zika J. D. (2017) Overturning in the Subpolar north Atlantic program: A new international ocean observing system. *Bull. Am. Meteorol. Soc.* **98**, 737–752.
- Macdonald R. W. and Gobeil C. (2012) Manganese Sources and Sinks in the Arctic Ocean with Reference to Periodic Enrichments in Basin Sediments. *Aquat. Geochem.* **18**, 565–591.
- Madec G., Bourdallé-Badie R., Bouttier P.-A., Bricaud C., Bruciaferri D., Calvert D., Jérôme Chanut L., Clementi E., Coward A., Delrosso D., Ethé C., Flavoni S., Graham T., Harle J., Iovino D., Lea D., Lévy C., Lovato T., Martin N., Masson S., Mocavero S., Paul J., Rousset C., Storkey D., Storto A. and Vancoppenolle M. (2017) *NEMO ocean engine. Notes du Pôle de modélisation*. l'Institut Pierre-Simon Laplace (IPSL).
- Mahowald N. M., Hamilton D. S., Mackey K. R. M., Moore J. K., Baker A. R., Scanza R. A. and Zhang Y. (2018) Aerosol trace metal leaching and impacts on marine microorganisms. *Nat. Commun.* **9**, 2614.
- Marsay C. M., Kadko D., Landing W. M., Morton P. L., Summers B. A. and Buck C. S. (2018) Concentrations, provenance and flux of aerosol trace elements during US GEOTRACES Western Arctic cruise GN01. *Chem. Geol.* **502**, 1–14.
- Martiny A. C., Pham C. T. A., Primeau F. W., Vrugt J. A., Moore J. K., Levin S. A. and Lomas M. W. (2013) Strong latitudinal patterns in the elemental ratios of marine plankton and organic matter. *Nat. Geosci.* **6**, 279–283.
- McLaughlin F. A., Carmack E. C., Macdonald R. W., Melling H., Swift J. H., Wheeler P. A., Sherr B. F. and Sherr E. B. (2004) The joint roles of Pacific and Atlantic-origin waters in the Canada Basin, 1997–1998. *Deep. Res. Part I Oceanogr. Res. Pap.* **51**, 107–128.
- McLaughlin F. A., Shimada K., Carmack E. C., Itoh M. and Nishino S. (2005) The hydrography of the southern Canada Basin, 2002. *Polar Biol.* **28**, 182–189.
- Measures C. I. (1999) The role of entrained sediments in sea ice in the distribution of aluminium and iron in the surface waters of the Arctic Ocean. *Mar. Chem.* **68**, 59–70.
- Michel C., Hamilton J., Hansen E., Barber D., Reigstad M., Iacozza J., Seuthe L. and Niemi A. (2015) Arctic Ocean outflow shelves in the changing Arctic: A review and perspectives. *Prog. Oceanogr.* **139**, 66–88.
- Michel C., Ingram R. G. and Harris L. R. (2006) Variability in oceanographic and ecological processes in the Canadian Arctic Archipelago. *Prog. Oceanogr.* **71**, 379–401.
- Middag R., van Hulten M. M. P., Van Aken H. M., Rijkenberg M. J. A., Gerringa L. J. A., Laan P. and de Baar H. J. W. (2015) Dissolved aluminium in the ocean conveyor of the West Atlantic Ocean: Effects of the biological cycle, scavenging, sediment resuspension and hydrography. *Mar. Chem.* **177**, 69–86.
- Milne A., Schlosser C., Wake B. D., Achterberg E. P., Chance R., Baker A. R., Forryan A. and Lohan M. C. (2017) Particulate phases are key in controlling dissolved iron concentrations in the (sub)tropical North Atlantic. *Geophys. Res. Lett.* **44**, 2377–2387.
- Moffett J. W. (1997) The importance of microbial Mn oxidation in the upper ocean: A comparison of the Sargasso Sea and equatorial Pacific. *Deep. Res. Part I* **44**, 1277–1291.
- Morton P. L., Landing W. M., Shiller A. M., Moody A., Kelly T. D., Bizimis M., Donat J. R., De Carlo E. H. and Shacat J. (2019) Shelf inputs and lateral transport of Mn Co, and Ce in the western north pacific ocean. *Front. Mar. Sci.* **6**, 1–25.
- Noble A. E., Moran D. M., Allen A. E. and Saito M. A. (2013) Dissolved and particulate trace metal micronutrients under the McMurdo Sound seasonal sea ice: Basal sea ice communities as a capacitor for iron. *Front. Chem.* **1**, 1–18.
- Ohnemus D. C., Auro M. E., Sherrell R. M., Lagerström M., Morton P. L., Twining B. S., Rauschenberg S. and Lam P. J. (2014) Laboratory intercomparison of marine particulate digestions including Piranha: a novel chemical method for dissolution of polyethersulfone filters. *Limnology and Oceanography: Methods* **12**(8), 530–547.
- Ohnemus D. C. and Lam P. J. (2015) Cycling of lithogenic marine particles in the US GEOTRACES North Atlantic transect. *Deep. Res. Part II* **116**, 283–302.
- Ohnemus D. C., Rauschenberg S., Cutter G. A., Fitzsimmons J. N., Sherrell R. M. and Twining B. S. (2017) Elevated trace metal content of prokaryotic communities associated with marine oxygen deficient zones. *Limnol. Oceanogr.* **62**, 3–25.
- Oldham V. E., Jones M. R., Tebo B. M. and Luther G. W. (2017) Oxidative and reductive processes contributing to manganese cycling at oxic-anoxic interfaces. *Mar. Chem.* **195**, 122–128.
- Proshutinsky A., Krishfield R., Timmermans M.-L., Toole J., Carmack E. C., McLaughlin F. A., Williams W. J., Zimmermann S., Itoh M. and Shimada K. (2009) Beaufort Gyre freshwater reservoir: State and variability from observations. *J. Geophys. Res.* **114**, C00A10.
- Rogalla B., Allen S. E., Colombo M., Myers P. G. and Oriens K. J. (2021) Sediments in sea ice drive the Canada Basin surface Mn maximum: insights from an Arctic Mn ocean model. *Earth Sp. Sci. Open Arch.*, 1–52.
- Rudnick R. L. and Gao S. (2013) *Composition of the Continental Crust*, second ed. Elsevier Ltd..
- Shaw D. M., Cramer J. J., Higgins M. D. and Truscott M. G. (2008) Composition of the Canadian Precambrian shield and the continental crust of the earth. *Geol. Soc. London Spec. Publ.* **24**, 275–282.
- Shelley R. U., Landing W. M., Ussher S. J., Planquette H. and Sarthou G. (2018) Regional trends in the fractional solubility of Fe and other metals from North Atlantic aerosols (GEOTRACES cruises GA01 and GA03) following a two-stage leach. *Biogeosciences* **15**, 2271–2288.
- Shimada K., Itoh M., Nishino S., McLaughlin F. A., Carmack E. C. and Proshutinsky A. (2005) Halocline structure in the Canada Basin of the Arctic Ocean. *Geophys. Res. Lett.* **32**, 1–5.
- Smethie W. M., Schlosser P., Bönsch G. and Hopkins T. S. (2000) Renewal and circulation of intermediate waters in the Canadian Basin observed on the SCICEX 96 cruise. *J. Geophys. Res. Ocean.* **105**, 1105–1121.

- Steele M., Morison J., Ermold W., Rigor I., Ortmeyer M. and Shimada K. (2004) Circulation of summer Pacific halocline water in the Arctic Ocean. *J. Geophys. Res.* **109**, 1–18.
- Sunda W. G. and Huntsman S. A. (1990) Diel cycles in microbial manganese oxidation and manganese redox speciation in coastal waters of the Bahama Islands. *Limnol. Oceanogr.* **35**, 325–338.
- Sunda W. G. and Huntsman S. A. (1988) Effect of sunlight on redox cycles of manganese in the southwestern Sargasso Sea. *Deep Sea Res. Part A Oceanogr. Res. Pap.* **35**, 1297–1317.
- Tang C. C. L., Ross C. K., Yao T., Petrie B., DeTracey B. M. and Dunlap E. (2004) The circulation, water masses and sea-ice of Baffin Bay. *Prog. Oceanogr.* **63**, 183–228.
- Taylor R. L., Semeniuk D. M., Payne C. D., Zhou J., Tremblay J.-É., Cullen J. T. and Maldonado M. T. (2013) Colimitation by light, nitrate, and iron in the Beaufort Sea in late summer. *J. Geophys. Res. Ocean.* **118**, 3260–3277.
- Thuróczy C. E., Gerringa L. J. A., Klunder M., Laan P., Le Guitton M. and De Baar H. J. W. (2011) Distinct trends in the speciation of iron between the shallow shelf seas and the deep basins of the Arctic Ocean. *J. Geophys. Res. Ocean.* **116**, 1–21.
- Timmermans M. L., Garrett C. and Carmack E. C. (2003) The thermohaline structure and evolution of the deep waters in the Canada Basin, Arctic Ocean. *Deep. Res. Part I Oceanogr. Res. Pap.* **50**, 1305–1321.
- Timmermans M. L., Marshall J., Proshutinsky A. and Scott J. (2017) Seasonally derived components of the Canada Basin halocline. *Geophys. Res. Lett.* **44**, 5008–5015.
- Tovar-Sánchez A., Duarte C. M., Alonso J. C., Lacorte S., Tauler R. and Galban-Malagón C. (2010) Impacts of metals and nutrients released from melting multiyear Arctic sea ice. *J. Geophys. Res. Ocean.* **115**, 1–7.
- Tremblay J.-É. and Gagnon J. (2009) The effects of irradiance and nutrient supply on the productivity of Arctic waters: a perspective on climate change. In *Influence of Climate Change on the Changing Arctic and Sub-Arctic Conditions*, pp. 73–93.
- Tremblay J.-É., Simpson K., Martin J., Miller L., Gratton Y., Barber D. and Price N. M. (2008) Vertical stability and the annual dynamics of nutrients and chlorophyll fluorescence in the coastal, southeast Beaufort Sea. *J. Geophys. Res. Ocean.* **113**, 1–14.
- Trimble S. M. and Baskaran M. (2005) The role of suspended particulate matter in 234Th scavenging and 234Th-derived export fluxes of POC in the Canada Basin of the Arctic Ocean. *Mar. Chem.* **96**, 1–19.
- Twining B. S., Rauschenberg S., Morton P. L. and Vogt S. (2015) Metal contents of phytoplankton and labile particulate material in the North Atlantic Ocean. *Prog. Oceanogr.* **137**, 261–283.
- Varela D. E., Crawford D. W., Wrohan I. A., Wyatt S. N. and Carmack E. C. (2013) Pelagic primary productivity and upper ocean nutrient dynamics across Subarctic and Arctic Seas. *J. Geophys. Res. Ocean.* **118**, 7132–7152.
- Vieira L. H., Achterberg E. P., Scholten J., Beck A. J., Liebetrau V., Mills M. M. and Arrigo K. R. (2019) Benthic fluxes of trace metals in the Chukchi Sea and their transport into the Arctic Ocean. *Mar. Chem.* **208**, 43–55.
- Walsh E. A., Kirkpatrick J. B., Rutherford S. D., Smith D. C., Sogin M. and D'Hondt S. (2016) Bacterial diversity and community composition from seafloor to subsurface. *ISME J.* **10**, 979–989.
- Wang Q., Myers P. G., Hu X. and Bush A. B. G. (2012) Flow constraints on pathways through the Canadian Arctic archipelago. *Atmos. - Ocean* **50**, 373–385.
- Wang X. H. (2002) Tide-induced sediment resuspension and the bottom boundary layer in an idealized estuary with a muddy bed. *J. Phys. Oceanogr.* **32**, 3113–3131.
- Whitmore L. M., Morton P. L., Twining B. S. and Shiller A. M. (2019) Vanadium cycling in the Western Arctic Ocean is influenced by shelf-basin connectivity. *Mar. Chem.* **216**.
- Woodgate R. A. and Aagaard K. (2005) Revising the Bering Strait freshwater flux into the Arctic Ocean. *Geophys. Res. Lett.* **32**, 1–4.
- Wright M. H., Geszvain K., Oldham V. E., Luther G. W. and Tebo B. M. (2018) Oxidative formation and removal of complexed Mn(III) by pseudomonas species. *Front. Microbiol.* **9**, 1–11.
- Wyatt S. N., Crawford D. W., Wrohan I. A. and Varela D. E. (2013) Distribution and composition of suspended biogenic particles in surface waters across Subarctic and Arctic seas. *J. Geophys. Res. Ocean.* **118**, 6867–6880.
- Xiang Y. and Lam P. J. (2020) Size-Fractionated Compositions of Marine Suspended Particles in the Western Arctic Ocean: Lateral and Vertical Sources. *J. Geophys. Res. Ocean.* **125**, 1–33.
- Yashayaev I., Bersch M. and van Aken H. M. (2007) Spreading of the Labrador Sea Water to the Irminger and Iceland basins. *Geophys. Res. Lett.* **34**, 1–8.
- Yashayaev I. and Clarke A. (2008) Evolution of North Atlantic Water Masses Inferred from Labrador Sea Salinity Series. *Oceanography* **21**, 30–45.
- Yashayaev I. and Loder J. W. (2009) Enhanced production of Labrador Sea Water in 2008. *Geophys. Res. Lett.* **36**, L01606.
- Yashayaev I. and Loder J. W. (2016) Recurrent replenishment of Labrador Sea Water and associated decadal-scale variability. *J. Geophys. Res. Ocean.* **121**, 8095–8114.
- Yigiterhan O., Murray J. W., Tugrul S. and Tu S. (2011) Trace metal composition of suspended particulate matter in the water column of the Black Sea. *Mar. Chem.* **126**, 207–228.
- Zakharova Y. R., Parfenova V. V., Granina L. Z., Kravchenko O. S. and Zemskaya T. I. (2010) Distribution of iron- and manganese-oxidizing bacteria in the bottom sediments of Lake Baikal. *Inl. Water Biol.* **3**, 313–321.
- Zinger L., Amaral-Zettler L. A., Fuhrman J. A., Horner-Devine M. C., Huse S. M., Welch D. B. M., Martiny J. B. H., Sogin M., Boetius A. and Ramette A. (2011) Global patterns of bacterial beta-diversity in seafloor and seawater ecosystems. *PLoS One* **6**, 1–12.

Associate editor: Karen Johannesson